



Combined Spectroscopic and Quantum Chemical Study of [trans-Ru(C≡CC₆H₄R¹-4)₂(dppe)₂]ⁿ⁺ and [trans-Ru(C≡CC₆H₄R¹-4)(C≡CC₆H₄R²-4)(dppe)₂]ⁿ⁺ (*n* = 0, 1) Complexes: Interpretations beyond the Lowest Energy Conformer Paradigm

Santiago Marqués-González,[†] Matthias Parthey,[‡] Dmitry S. Yufit,[†] Judith A. K. Howard,[†] Martin Kaupp,^{*,‡} and Paul J. Low^{*,§}

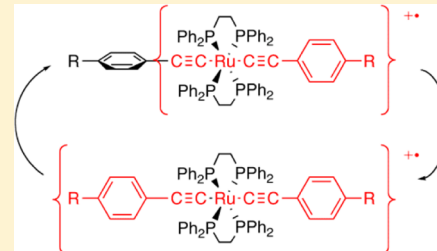
[†]Department of Chemistry, Durham University, South Road, DH1 3LE Durham, U.K.

[‡]Institut für Chemie Sekr. C7, Technische Universität Berlin, Strasse des 17. Juni 135, 10623 Berlin, Germany

[§]School of Chemistry and Biochemistry, University of Western Australia, 35 Stirling Highway, Crawley, 6009 Perth, Australia

Supporting Information

ABSTRACT: The reaction of *trans*-RuCl(C≡CC₆H₄R¹-4)(dppe)₂ (2; R¹ = Me (a), C₅H₁₁ (b), OMe (c), CO₂Me (d), NO₂ (e), C≡CSiMe₃ (f), C≡CBu^t (g), NH₂ (h)), prepared *in situ* from reactions of [RuCl(dppe)₂]OTf ([1]OTf) with terminal alkynes in CH₂Cl₂ solutions containing 1,8-diazabicycloundec-7-ene (DBU) and TiBF₄, provides a convenient and rapid route to bis(acetylide) complexes *trans*-Ru(C≡CC₆H₄R¹-4)₂(dppe)₂ (3a–h) and *trans*-Ru(C≡CC₆H₄R¹-4)(C≡CC₆H₄R²-4)(dppe)₂ (4, R¹ = C≡CSiMe₃, R² = NH₂; 5, R¹ = CO₂Me, R² = NH₂; 6, R¹ = CO₂Me, R² = OMe). However, even in the absence of the chloride abstracting reagent, more strongly electron donating substituents (e.g., R¹ = OMe (2c), NH₂ (2h)) promote sufficient ionization of the Ru–Cl bond in *trans*-RuCl(C≡CC₆H₄R¹-4)(dppe)₂ to lead to slow conversion to bis(alkynyl) complexes 3c,h in the presence of excess alkyne and DBU. Desilylation of 2f and 3f affords 2i and 3i (R¹ = C≡CH), respectively. The molecular structures of 3a–d,f–i have been determined and are reported together with the structures of the monoalkynyl complexes 2f,g,i and compared with related compounds from the literature. Complexes 3a–i and 4–6 undergo one reversible electrochemical oxidation process, which can be attributed to depopulation of an orbital with significant alkynyl ligand character. The one-electron-oxidation products [3f]^{•+}, [3h]^{•+}, [4]^{•+}, and [5]^{•+}, chosen to serve as representative examples of this family of complexes, each exhibit a series of NIR absorptions between 15000 and 5000 cm^{−1} which on the basis of TDDFT calculations cannot be attributed to a single, static lowest energy molecular structure. Rather, the transitions that are responsible for the absorption band envelope have varying degrees of LMCT and inter-alkynyl ligand IVCT or MLCT character that depend not only on the nature of the Rⁿ groups but also on the ensemble of thermally populated molecular conformers in solution with various relative orientations of the metal fragment and arylethynyl moieties.



INTRODUCTION

The complexes *trans*-Ru(C≡CR)₂(dppe)₂ and differentially (or unsymmetrically) substituted derivatives *trans*-Ru(C≡CR)(C≡CR')(dppe)₂ are emerging as important structural and electronic moieties in a range of molecular electronic^{1–3} and electrooptic⁴ applications. These materials properties are due in no small part to the efficient mixing of the organic alkynyl π-electron system with the central metal d-orbitals, which gives rise to polymeric systems with highly delocalized electronic structures.⁵ One-pot methods for the preparation of the complexes *trans*-Ru(C≡CR)₂(dppe)₂ are often based on activation of *cis*-RuCl₂(dppe)₂ with NaPF₆ in the presence of the precursor alkyne and a suitable base, usually NEt₃, over reaction periods that can extend for several days (Scheme 1).^{6–9} The bis(alkynyl) complexes *trans*-Ru(C≡CR)₂(dppe)₂ may also be prepared in two steps via intermediate monoacetylide *trans*-RuCl(C≡CR)(dppe)₂ or vinylidene

[RuCl(C=CHR)(dppe)₂]⁺ complexes through a sequence of deprotonation (in the case of vinylidenes), halide abstraction, alkyne coordination, rearrangement, and deprotonation reactions (Scheme 1a).^{10,6,11,12} Alternatively, ammine complex intermediates, [Ru(C≡CR)(NH₃)(dppe)₂]⁺, which can be prepared from either *trans*-RuCl(C≡CR)(dppe)₂, NH₄PF₆, and NEt₃ (Scheme 1b)¹³ or *trans*-Ru(C≡CR)₂(dppe)₂ and NH₄PF₆ (Scheme 1c),¹⁴ may be employed as precursors to *trans*-bis(alkynyl) complexes, including differentially (or unsymmetrically) substituted derivatives (Scheme 1d),¹⁴ and Os analogues.¹³

Here we report further developments in synthetic routes to the complexes *trans*-Ru(C≡CC₆H₄R¹-4)₂(dppe)₂ and *trans*-

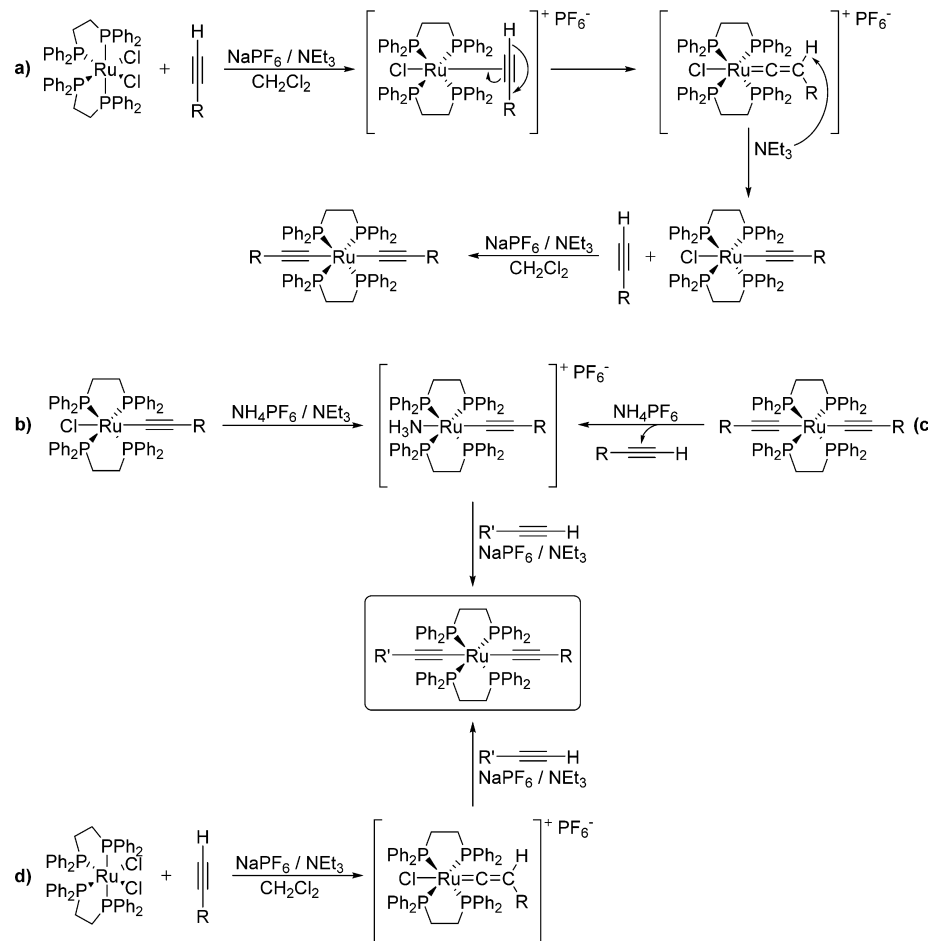
Special Issue: Organometallic Electrochemistry

Received: March 12, 2014

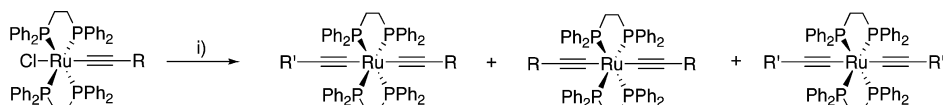
Published: July 3, 2014



Scheme 1. Conceptual Steps in the Preparation of (a) *trans*-Ru(C≡CR)₂(dppe)₂ from *cis*-RuCl₂(dppe)₂, (b) *trans*-Ru(C≡CR)(C≡CR')(dppe)₂ from *trans*-RuCl(C≡R)(dppe)₂ via Intermediate Ammine Complexes, (c) *trans*-Ru(C≡CR)(C≡CR')(dppe)₂ from *trans*-Ru(C≡R)₂(dppe)₂ via Intermediate Ammine Complexes, and (d) *trans*-Ru(C≡CR)(C≡CR')(dppe)₂ via Intermediate Vinylidene Complexes [RuCl(C=CHR)₂]PF₆



Scheme 2. Ligand Scrambling over Long Reaction Times Leading to Symmetrical and Unsymmetrical Bis(alkynyl) Complexes^a



^aLegend: (i) HC≡CR', NEt₃, NaPF₆.

Ru(C≡CC₆H₄R¹-4)(C≡CC₆H₄R²-4)(dppe)₂. A combination of spectroelectrochemical (UV-vis/NIR) and computational (DFT/TDDFT) methods have been used to explore the electronic structure of these species, with the oxidation leading to more or less highly delocalized radical cations, the precise distribution of spin density within which is highly dependent on the relative conformation of the metal center and alkynyl ligand substituents.

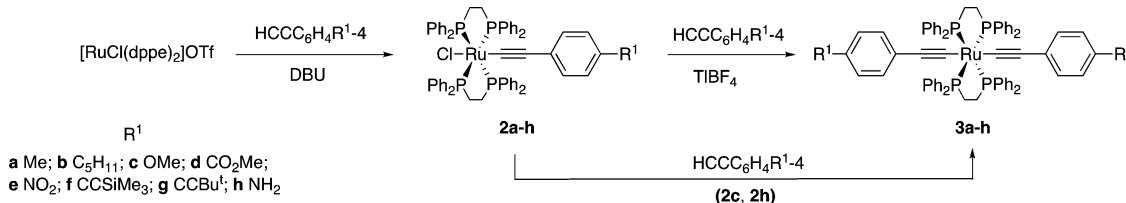
RESULTS AND DISCUSSION

Synthetic Studies. The complex *trans*-RuCl₂(dppe)₂ is relatively inert to substitution reactions, due to the limited lability of the chloride ligands,¹⁵ and preparations of *trans*-Ru(C≡CR)₂(dppe)₂ complexes from this precursor are generally restricted to transmetalation strategies using trimethyltin alkynes and CuI catalysts.¹⁶ In contrast, one chloride ligand in *cis*-RuCl₂(dppe)₂ is more labile due to the stronger

trans effect of the phosphine ligands. In the presence of a suitable halide abstracting agent, such as NaPF₆, reactions of *cis*-RuCl₂(dppe)₂ with 1-alkynes, HC≡CR, proceed to give the corresponding vinylidene *trans*-[RuCl(C=CHR)(dppe)₂]⁺ (Scheme 1a).¹² The strongly electron withdrawing nature of the vinylidene ligand decreases the lability of the remaining chloride, allowing ready isolation of the monovinylidene compounds. The reaction of the five-coordinate complex [RuCl(dppe)₂]OTf (**1**) with 1-alkynes, HC≡CR, is also now well-known to rapidly give the corresponding vinylidene complexes *trans*-[RuCl(C=CHR)(dppe)₂]⁺.^{11,17,18}

Deprotonation of *trans*-[RuCl(C=CHR)(dppe)₂]⁺ gives the alkynyl complexes *trans*-RuCl(C≡CR)(dppe)₂, with the stronger *trans* effect of the alkynyl ligand again leading to an increase in lability of the chloride ligand and permitting access to bis(alkynyl) complexes (Scheme 1a).¹⁹ In our hands, efforts to prepare unsymmetrical substituted complexes *trans*-[Ru(C≡

Scheme 3. Synthesis of Symmetrically Substituted Complexes 3a–h



CR)(C≡CR')(dppe)₂] are often complicated by ligand scrambling leading to mixtures of symmetric and unsymmetric products (Scheme 2), and similar difficulties have been noted in analogous dppm systems.^{20,21} The reversibility of the sequence of reactions shown in Scheme 1d might account for the modest yields of the unsymmetrical complexes often reported.¹⁹ These complications can be avoided to some extent through the use of transmetalation-based synthetic strategies,¹⁶ or through the use of activated alkynyl ammine complexes¹⁴ and reaction media containing a strong, non-nucleophilic base to minimize the accumulation of vinylidene intermediates.¹¹ We have now directed attention to the factors influencing the lability of the chloride ligand in *trans*-RuCl(C≡CR)(dppe)₂ complexes (2) with a view to developing a rapid method for the preparation of symmetrical (3) and unsymmetrical (4–6) bis(alkynyl) complexes.

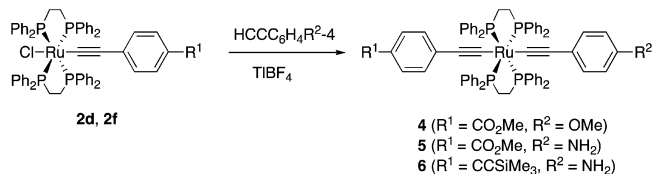
Treatment of [RuCl(dppe)₂]OTf ([1]OTf) with an excess of a 1-alkyne and DBU in CH₂Cl₂ gave yellow solutions of the alkynyl complexes *trans*-RuCl(C≡CC₆H₄R¹-4)(dppe)₂, over ca. 30 min (2a–h; Scheme 3), which were isolated by way of example for 2d–g (2a,e²² and 2f^{1,23} already having been prepared by closely related routes), while treatment of 2f with tetrabutylammonium fluoride afforded 2i.^{24,25} Spectroscopic (³¹P NMR) analysis detected trace amounts of the bis(alkynyl) complexes 3 (vide infra) as barely discernible resonances near 54 ppm (see the Supporting Information). However, the solutions of 2a–h prepared *in situ* proved to be efficient entry points to bis(alkynyl) complexes. Spectroscopic (³¹P NMR) analysis detected trace amounts of the bis(alkynyl) complexes 3 (vide infra) as barely discernible resonances near 54 ppm (see the Supporting Information).

Addition of TiBF₄ to solutions of 2a–h prepared from [1]OTf and just over 2 equiv of terminal alkyne resulted in precipitation of TlCl and formation of the symmetric complexes *trans*-[Ru(C≡CC₆H₄R-4)₂(dppe)₂] (3a,¹⁵ 3b–d, 3e,¹⁵ 3f,g,²⁶ 3h; Scheme 3). Desilylation (NBu₄F) of 3f gave 3i²⁷ in good yield. In most instances, a careful filtration proved sufficient to remove the TlCl and protonated DBU salts from the reaction mixture, with subsequent precipitation of the bis(alkynyl) complexes 3a–d,f,g from the reaction mixture being achieved by addition of the appropriate solvent (see the Experimental Section). Any remaining trace quantities of unreacted mono(alkynyl) complexes were evinced in the ³¹P NMR spectra as singlets near 49 ppm. However, the addition of Tl⁺ salts did not drive the reaction of [1]OTf with 2 equiv of 1-ethynyl-4-nitrobenzene to completion, yielding instead a mixture of mono- (2e) and bis(alkynyl) (3e) complexes over 48 h. While the use of NaPF₆ in the presence of NEt₃ allows further substitution of the chloride ligand in 2c,²⁸ surprisingly the Tl⁺ salts proved less effective in this context. In addition, the poor solubility of 3e hindered further chromatographic purification, reducing the final yield to ca. 15%. Also, while the addition of TiBF₄ to a mixture of 2h, DBU, and HC≡

CC₆H₄NH₂ gave *trans*-Ru(C≡CC₆H₄NH₂-4)₂(dppe)₂ (3h) in high yield (as judged by *in situ* monitoring of the reaction by NMR spectroscopy), any attempt to purify the final product from the reaction mixture led to decomposition.

As described above, treatment of a CH₂Cl₂ solution of [RuCl(dppe)₂]OTf ([1]OTf) with an excess of 4-ethynylaniline or 4-ethynylaniline and DBU gave yellow solutions of the alkynyl complexes *trans*-RuCl(C≡CC₆H₄OMe-4)(dppe)₂ (2c) and *trans*-RuCl(C≡CC₆H₄NH₂-4)(dppe)₂ (2h), respectively (Scheme 3).¹⁷ Over the course of 7 days, and without the addition of halide abstracting agents, the reaction solutions deposited a precipitate of pure bis(alkynyl) complexes *trans*-Ru(C≡CC₆H₄OMe-4)₂(dppe)₂ (3c) and *trans*-Ru(C≡CC₆H₄NH₂-4)₂(dppe)₂ (3h) in ca. 45% isolated yield. Similar reactions of complexes 2 prepared from 1-alkynes bearing less electron donating substituents or electron withdrawing groups did not proceed to give bis(alkynyl) complexes 3 to any synthetically useful extent in the absence of additional reagents. Clearly, the trans effect of the alkynyl ligands bearing electron-donating groups plays a significant role in activating the chloride ligand in 2c,h toward substitution.

In spite of these exceptions, the reaction sequence described above can be adapted to permit the rapid formation of unsymmetrically substituted complexes *trans*-Ru(C≡CC₆H₄R¹-4)(C≡CC₆H₄R²-4)(dppe)₂ in expeditious fashion (Scheme 4). Treatment of a CH₂Cl₂ solution of the appropriate

Scheme 4. Synthesis of Unsymmetrically Substituted Complexes 4–6 from 2d,f using Tl⁺ as Halide Abstracting Agent

mono(alkynyl) complexes *trans*-RuCl(C≡CC₆H₄R¹-4)(dppe)₂ (2d,f) and excess DBU with 1 equiv of TiBF₄ and subsequent dropwise addition of a terminal alkyne HC≡CR² over 30 min generated an off-white precipitate (TlCl). Simple filtration to remove the precipitated salts gave filtrates containing *trans*-Ru(C≡CC₆H₄R¹-4)(C≡CC₆H₄R²-4)(dppe)₂ (4, R¹ = C≡CCSiMe₃, R² = NH₂; 5, R¹ = CO₂Me, R² = NH₂; 6, R¹ = CO₂Me, R² = OMe), which were obtained as pure powders in moderate to good yield upon addition of hexane (Scheme 4).

Crystallographic Studies. The structures of the bis(alkynyl) complexes 3a,¹⁵ 3b–d, 3f,²⁶ 3g,²⁶ 3h, and 3i²⁷ were determined by single-crystal X-ray diffraction, together with those of the mono(alkynyl) species 2f,²³ 2g, and 2i.^{24,25} Single crystals of the unsymmetrically substituted complexes 4–6 were found to be disordered, impeding conclusive identification of the alkynyl substituents. Representative molecular plots and

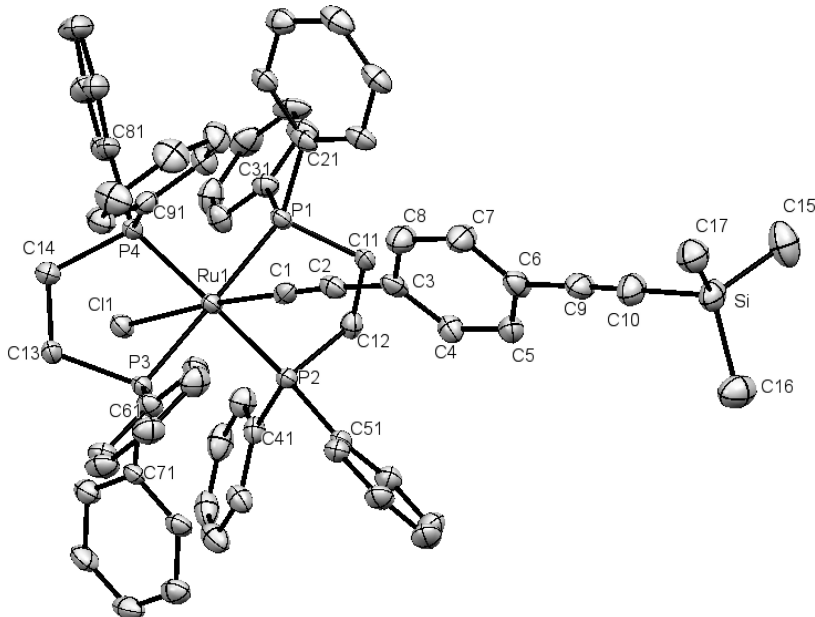


Figure 1. Plot of a molecule of $\text{trans-RuCl}(\text{C}\equiv\text{CC}_6\text{H}_4\text{C}\equiv\text{CSiMe}_3\text{-}4)_2(\text{dppe})_2$ (**2f**) with thermal ellipsoids at the 50% probability level. Solvent molecules and hydrogen atoms have been omitted for clarity.

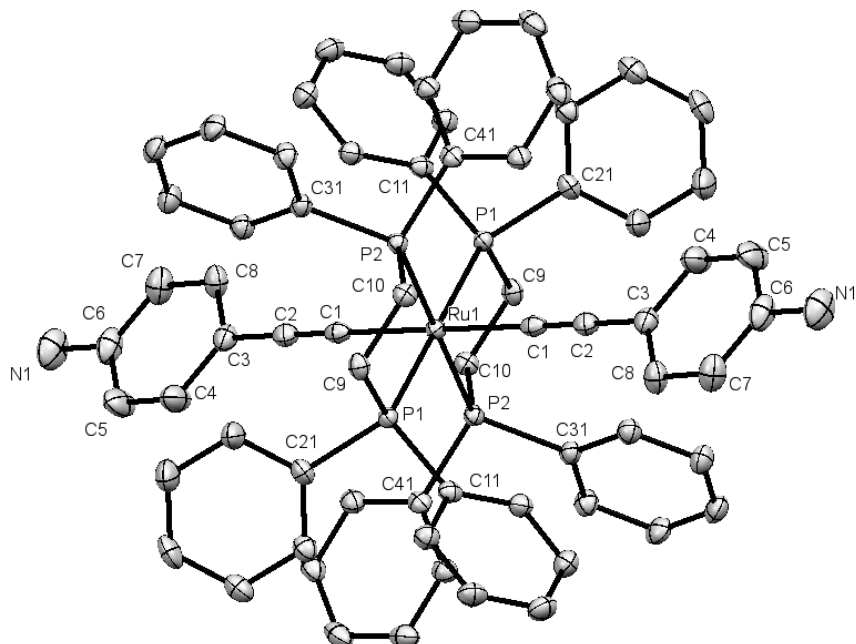


Figure 2. Plot of a molecule of $\text{trans-Ru}(\text{C}\equiv\text{CC}_6\text{H}_4\text{NH}_2\text{-}4)_2(\text{dppe})_2$ (**3h**) with thermal ellipsoids at the 50% probability level. Hydrogen atoms have been omitted for clarity.

atom labeling schemes are given in Figures 1 (**2f**) and 2 (**3h**), while key bond lengths (Å) and angles (deg) are given in Tables 1 and 2 for these complexes and related systems for comparison. Crystallographic data and more extensive lists of bond lengths and angles are summarized in the Supporting Information, together with figures illustrating all of the molecular structures reported here.

All the complexes adopt an approximately octahedral environment at the Ru center, with small distortions arising from the constrained bite angle of the dppe ligands. Although the experimental evidence shows that chloride substitution in $\text{trans-RuCl}(\text{C}\equiv\text{CR})(\text{dppe})_2$ is clearly influenced by the electronic character of the alkynyl ligand, there is little evidence

for a closely correlated structural trans effect (Table 1). At first inspection, complexes such as $\text{trans-RuCl}(\text{C}\equiv\text{CC}_6\text{H}_4\text{NPh}_2)\text{-}(\text{dppe})_2$ and **2c** bearing electron-donating groups display elongated Ru–Cl bond lengths, consistent with the electron-donating ability of the alkynyl ligand located trans to chloride. Similarly, at the opposite end of the table, shorter Ru–Cl bond lengths can be found associated with complexes featuring trans alkynyl ligands bearing electron-withdrawing substituents such as $\text{trans-RuCl}\{\text{C}\equiv\text{CC}_6\text{H}_3(\text{Me}-2)\text{NO}_2\text{-}4\}\text{(dppe)}_2$ and **2d**. These structural features, which reflect the π -donor properties of the chloride ligand and π -donor/weak π -acceptor character of the alkynyl ligand, are in agreement with the synthetic

Table 1. Selected Bond Lengths (Å) from Crystallographically Characterized Complexes *trans*-RuCl(C≡CR)(dppe)₂

R	Ru-Cl	Ru-C≡C	C≡C	Ru-P _{avg}	θ (°)	Ref
C ₆ H ₃ (Me-2)NO ₂ -4 C ₆ H ₅	2.473(3) 2.4786(13)	2.013(11) 2.007(5)	1.189(14) 1.198(7)	2.386 2.371	2 7	¹⁵ ⁹
C ₆ H ₄ C≡CBu ^t (2g)	2.4799(11)	1.997(4)	1.234(5)	2.369	75	this work
C ₆ H ₄ CO ₂ Me (2d)	2.4806(13)	1.998(5)	1.195(8)	2.368	92	¹⁷
C ₆ H ₄ -C ₃ N ₃ (NHCOEt) ₂	2.4811(10)	1.988(4)	1.221(5)	2.372	74	²⁹
C ₆ H ₄ C(=O)Me-4	2.4831(11)	1.989(4)	1.212(6)	2.3685	92	³⁰
C ₆ H ₄ -C ₃ N ₃ (NHC ₂ Bu ^t) ₂	2.4832(9)	1.996(4)	1.204(5)	2.362	72	²⁹
C ₅ H ₃ NC ₅ H ₄ N	2.4871(15)	2.007(6)	1.183(8)	2.367	88	²⁰
C ₆ H ₄ CH=CHC ₆ H ₄ NO ₂	2.489(1)	1.996(4)	1.205(7)	2.368	26	³¹
C ₆ H ₄ Me-0.5THF (2a)	2.4907(12)	2.009(5)	1.196(6)	2.360	12	¹⁷
C ₅ H ₃ NC ₅ H ₄ N.PdCl ₂	2.4988(13)	1.969(5)	1.235(7)	2.368	6	²⁰
C ₆ H ₄ NO ₂ -4 (2e)	2.500(1)	1.986(5)	1.206(7)	2.366	66	¹⁵
C ₆ H ₄ C≡CH (2i)	2.50030(6)	2.027(2)	1.190(3)	2.3879	59	this work
C ₆ H ₄ C≡CSiMe ₃ (2f)	2.5041(11)	2.005(5)	1.196(6)	2.359	4	this work
C ₆ H ₄ C(=O)H	2.507(1)	2.012(4)	1.158(5)	2.377	65	³¹
C ₆ H ₄ Me-2CH ₂ Cl ₂ (2a)	2.5096(8)	2.007(4)	1.202(5)	2.369	64	¹⁷
C ₄ H ₂ SCH=C ₄ H ₂ SC(=O)H	2.5099(10)	1.990(4)	1.197(5)	2.379	78	³²
C ₆ H ₄ OMe (2d)	2.5118(9)	2.018(4)	1.188(5)	2.369	65	¹⁷
C ₆ H ₄ F-4	2.5149(10)	2.013(4)	1.197(5)	2.371	51	³³
C ₆ H ₄ NPh ₂	2.5349(7)	1.997(3)	1.215(4)	2.366	90	³⁴
C ₆ H ₄ F-3	2.5370(18)	2.043(8)	1.096(9)	2.376	14	¹⁰
H (CCH/Cl disorder 50:50 occupancy)	2.5838(14)	1.936(5)	1.190(5)	2.367	---	³⁵

Table 2. Selected Bond Lengths (Å) from Crystallographically Characterized Complexes *trans*-Ru(C≡CR)(C≡CR')(dppe)₂

R	R'	Ru-C≡CR	Ru-C≡CR'	C≡C	Ru-P _{avg}	θ (°)	REF
C{CH=C(CN) ₂ }≡C(CN) ₂	C{CH=C(CN) ₂ }≡C(CN) ₂	2.007(7)		1.231(9)	2.389	---	²¹
C ₆ H ₂ (OMe) ₂ C≡CH	C ₆ H ₂ (OMe) ₂ C≡CH	2.047(5)		1.223(6)	2.352	2	²²
C≡CH	C≡CH	2.050(4)		1.198(5)	2.369	---	²³
C ₆ H ₄ C≡CBu ^t	C ₆ H ₄ C≡CBu ^t	2.057(2)		1.211(3)	2.358	65	(3g)
C ₆ H ₂ (OMe) ₂ C≡CSiMe ₃	C ₆ H ₂ (OMe) ₂ C≡CSiMe ₃	2.0583(17)		1.218(2)	2.357	17	²²
C ₆ H ₄ C≡CH (mol A)	C ₆ H ₄ C≡CH	2.061(3)		1.212(4)	2.357	55	(3i)
C ₆ H ₅	C ₆ H ₅	2.061(5)	2.064(5)	1.207(7)	2.360	0/58	⁹
C ₆ H ₅	C ₆ H ₄ C(=O)H (disordered)	2.0619(19)		1.213(3)	2.363	75	²⁴
C ₆ H ₄ C≡CH (mol B)	C ₆ H ₄ C≡CH	2.062(3)		1.209(4)	2.354	82	(3i)
C ₆ H ₅	C ₆ H ₄ C≡C{Fe(dppe)Cp*} ⁺	2.063(5)	2.062(5)	1.2096(6)/1.201(6)	2.369	60/60	²⁵
C ₆ H ₄ OMe	C ₆ H ₄ OMe	2.0648(16)		1.217(2)	2.358	70	(3e)
C ₆ H ₄ Me-4	C ₆ H ₄ Me-4	2.065(2)		1.210(3)	2.349	68	(3a)
C ₆ H ₄ C≡CSiMe ₃	C ₆ H ₄ C≡CSiMe ₃	2.066(3)		1.204(4)	2.358	68	(3f)26
C ₆ H ₅ C ₅ H ₁₁ -4	C ₆ H ₅ C ₅ H ₁₁ -4	2.0666(16)		1.206(2)	2.355	59	(3b)
C ₆ H ₄ CO ₂ Me	C ₆ H ₄ CO ₂ Me	2.0687(18)		1.197(2)	2.357	64	(3d)
TTFMe ₃	TTFMe ₃	2.0691(18)		1.203(3)	2.373	13	²⁷
C ₆ H ₄ NH ₂	C ₆ H ₄ NH ₂	2.074(2)		1.197(3)	2.349	64	(3h)
Fc	Fc	2.075(3)		1.212(5)	2.358	---	²⁸
Fc	C ₆ H ₄ NPh ₂	2.082(3)	2.061(3)	C≡CR ¹ : 1.213(4) C≡CR ² : 1.213(4)	2.356	---/86	¹⁹
C≡CSiMe ₃	C≡CSiMe ₃	2.095(14)		1.099(17)	2.360	---	²³
C ₆ H ₅	C ₅ H ₃ NC ₅ H ₄ N.Dyhfacac	2.105(7)	2.049(6)	1.118(9) 1.210(7)	2.350	5/45	²⁹

observations, where electron-donating ligands favor the substitution of the trans-disposed chloride.

However, Table 1 also contains several examples of mono(alkynyl) complexes for which the structural data are in disagreement with the reactivity profiles. For example, the complex *trans*-RuCl(C≡CC₆H₅)(dppe)₂ presents a Ru-Cl bond length (2.4786(13) Å) which is unexpectedly shorter than that of the most unreactive complex of the series, *trans*-RuCl(C≡CC₆H₃(Me-2)NO₂-4)(dppe)₂ (**2e**, 2.500(1) Å). On the other hand, the complex *trans*-RuCl{C≡CC₆H₃(Me-2)NO₂-4}(dppe)₂, which is closely related to **2e**, presents the shortest of the Ru-Cl bond lengths observed in Table 1 (2.473(3) Å). A further remarkable exception concerns the complex *trans*-RuCl(C≡CC₆H₄Me)(dppe)₂ (**2a**), which presents two substantially different Ru-Cl bond lengths depending on the nature of the solvate in the unit cell: 0.5THF, 2.4907(12) Å; 2CH₂Cl₂, 2.5096(8) Å.¹⁷

A closer analysis of the structural details of these complexes revealed that for the complex *trans*-RuCl(C≡CC₆H₄Me)(dppe)₂·0.5THF (**2a**·0.5THF) the torsion angle between the plane of the arylethynyl ligand and the plane bisecting the dppe ligands, θ (Figure 3), is 12° while for *trans*-RuCl(C≡CC₆H₄Me)(dppe)₂·2CH₂Cl₂ θ = 64°. Previous computational studies revealed that the Ru-based d_{xz} and d_{yz} orbitals are involved in the HOMO of *trans*-RuCl(C≡CC₆H₄R)(dppe)₂ complexes³⁰ (taking the axial Ru-ethynyl vector as the z direction and x and y in the plane of the equatorial dppe ligands). Thus, a θ = 90 or 0° configuration of the aromatic portion of the alkynyl ligand (italicized entries in Table 1) provides better overlap of the arylethynyl ligand π and π* orbitals with respect to the metal center, enhancing the electronic influence of the ligand on the Ru-Cl bond length and giving rise to a consistent structure–property relationship. The structural parameters of complexes which offer θ values

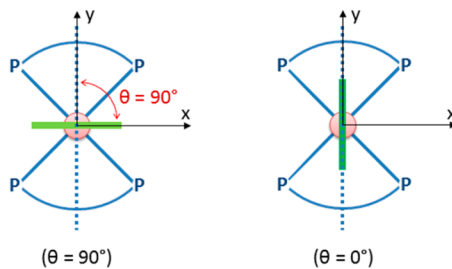


Figure 3. Representation of angle θ in *trans*-RuCl(C≡CC₆H₄R)(dppe)₂.

that deviate substantially from the optimal 0 or 90° conformations are less well correlated with the simple ideas of the structural trans effect based on the donor or acceptor properties of the alkynyl ligand substituent, due to the lack of extended conjugation between the substituent and the metal center.

The importance of the ligand orientation (expressed as the angle θ) is clearly illustrated by the contrasting molecular structures of the closely related complexes *trans*-RuCl(C≡CC₆H₄NO₂-4)(dppe)₂ (**2e**) and *trans*-RuCl{C≡CC₆H₃(Me-2)NO₂-4}(dppe)₂. Although the electronic properties of the ligands (4-nitrophenyl)ethynyl and (4-nitro-2-methylphenyl)-ethynyl should be essentially identical, the latter complex presents a much shorter Ru–Cl bond length (Table 1, 2.500(1) vs 2.473(3) Å). It appears from inspection of a space-filling model that the methyl group present in *trans*-RuCl{C≡CC₆H₃(Me-2)NO₂-4}(dppe)₂ locks into a groove formed by the dppe phenyl rings and forces the nitroaromatic moiety to adopt a $\theta = 2^\circ$ configuration, enhancing drastically the trans effect. On the other hand, the non sterically hindered C≡CC₆H₄NO₂-4 adopts a configuration in the crystal such that $\theta = 66^\circ$, which reduces the ligand influence on the trans-disposed chloride. The importance of ligand orientation and molecular conformation on molecular electronic structure is well-known, and dynamic changes in molecular conformation are becoming increasingly recognized as a contributing factor to solution-based spectroscopic properties (vide infra).³⁶ These observations are supported by the solid-state structure–property relationships summarized in Table 1.

The bis(alkynyl) complexes **3a–d,f–i** and other examples in Table 2 present a linear rodlike structure with angles along the –C≡C–Ru–C≡C– fragment close to 180° and the aryl rings of both alkynyl ligands lying in a common plane. In comparison to their monosubstituted counterparts **2**, the bis(alkynyl) complexes **3** generally exhibit longer Ru–C≡C bonds and correspondingly shorter Ru–P bond lengths (Table 2). In a manner similar to that described for the mono(alkynyl) complexes, a variety of θ angles from 0 to 90° can be found across the data set, but few near the optimal angles of 0 and 90°. Due to the importance of orbital overlap on the propagation of electronic effects through the molecular backbone, a systematic relationship between the electronic properties of the alkynyl ligand substituent and bond lengths cannot be found for these complexes, with θ angles that deviate from the optimal 0 and 90° positions. However, it appears that the greater σ - and π -donor properties of the additional alkynyl ligand in bis(alkynyl) complexes **3** vs the inductive electron-withdrawing and π -donor properties of the chloride ligand in complexes **2** leads to an increased amount of electron density at the metal center and a greater degree of π back-donation to the

phosphine ligands. This in turn leads to shorter Ru–P distances in the bis(alkynyl) complexes than in the mono(alkynyl) analogues.

Electrochemistry. The electrochemical response of *trans*-RuX(C≡CR)(dppe)₂ (X = Cl, C≡CR) complexes is summarized in Table 3, although comparisons with data

Table 3. Electrochemical Data from 2a–g,i, 3a–i, and 4–6^a

complex	E_1° (V)	E_2° (V)	E_3° (V)	E_4^{ox} (V)
2a ¹⁷	-0.03			0.85
2b ¹⁷	-0.04			0.83
2c ¹⁷	-0.10			0.69
2d ¹⁷	0.10			0.98
2e ¹⁷	0.20			1.10
2f ^{11,23}	0.04			0.98
2g	-0.01			0.85
2i ^{24,25}	0.06			0.90
3a ¹⁵	-0.06			0.85
3b	-0.09			0.80
3c	-0.15			0.65
3d	0.12			0.90
3e ¹⁵	0.26			
3f ²⁶	0.05			0.90
3g ²⁶	0.00			0.85
3h	-0.29	0.10	0.46	
3i ²⁷	0.05			0.90
4	-0.21	0.20		
5	-0.19	0.22		0.61
6	-0.04			0.76

^a $E_{1/2}^\circ$ vs ferrocene/ferrocenium (FeCp₂/[FeCp₂]⁺) (CH₂Cl₂, 0.1 M NBu₄BF₄, Pt-dot working electrode). Under these conditions, the internal reference decamethylferrocene/decamethylferrocenium (FeCp₂*₂/[FeCp₂*₂]⁺) appears at -0.53 V vs FeCp₂/[FeCp₂]⁺.

reported elsewhere are made difficult by the various combinations of solvent, electrolyte, and reference potential employed in these earlier works. As previously reported in earlier studies of similar complexes, a reversible first oxidation process E_1° was present in almost every case,^{6,11,13,15,17,38,45} although the poor solubility of **3e** prevented the recording of accurate voltammetric data in common solvents. One or two additional oxidation processes (E_2°, E_3°) were found for amino-substituted complexes **3h**, **4**, and **5**. The low oxidation potential of **3i** provides a reasonable explanation for the experimental difficulties found during workup. In most cases an irreversible, multielectron oxidation wave E_4 was also present close to the anodic solvent limit (Table 3).

The range of potentials E_1° recorded for compounds **2a–g,i** and **3a–i** span from 300 mV to over 500 mV, respectively. The correlation of the electronic character of the remote substituents on the redox properties of the complexes is consistent with a strong arylacetylidyne character of the HOMO^{5,46} and the greater conformational freedom offered by the solution medium as opposed to the solid state that permits better π conjugation in the molecular backbone. Not unexpectedly, complexes **2c** and **3c,h**, which bear the most electron donating aryl substituents, were more easily oxidized in the thermodynamic sense than other members of the series, while the oxidation of **2d** and **3d,e**, which bear electron-withdrawing substituents, required considerably more positive potentials. In comparison to their monosubstituted partners, only slight variations were found in the electrochemical

properties of the bis(alkynyl) complexes. According to Lever's early model, the influence of different ligands on the electronic properties of a coordination complex is frequently found to be additive.⁴⁷ However, Heath and Humphrey reported an attenuation of those additive effects for complexes bearing trans-disposed π -accepting ligands.^{48,49} Lever's model is able to accurately predict the influence of a ligand on the electronic properties of a coordination complex when the oxidation process is located on the metal center. Hence, alkynyl complexes of Os and Ru, which present a characteristic and pronounced ligand contribution to the HOMO (vide infra), often deviate from the predictions of the Lever model,⁵⁰ and this is particularly relevant to complexes bearing redox-active ligands in which the metallic nature of the redox processes is far from clearly established.

Spectroelectrochemistry and Quantum Chemical Calculations. Although complexes *trans*-RuX(C \equiv CR)-dppe₂ have been the subject of UV-vis/NIR spectroelectrochemical studies,^{28,30,51,52} the use of IR spectroelectrochemical methods to study this class of compounds is relatively rare,^{38,53} despite the considerable amount of complementary electronic and chemical structural detail contained in the IR spectroelectrochemical response of alkynyl complexes.⁵⁴ Here we present an IR spectroelectrochemical study of compounds 3c,f,h and 4–6, together with comparable UV-vis/NIR spectroelectrochemical studies of the unsymmetrically substituted complexes 4 and 5 with reference data from 3f,h. These complexes were selected because of their demonstrated (3f), or potential (3h, 4), capacity to perform as wires during single-molecule conductance measurements²⁶ or to serve as reference compounds with different electron-donating groups (3c) or vibrational probes (5 and 6). To gain further insight into the electronic structure, density functional theory (DFT) calculations were performed on [3f]ⁿ⁺, [3h]ⁿ⁺, [4]ⁿ⁺, and [5]ⁿ⁺ ($n = 0, 1$).

Molecular and electronic structural changes upon oxidation were followed by key IR vibrational modes, such as $\nu(\text{RuC}\equiv\text{C})$ and the noncoordinated $\nu(\text{C}\equiv\text{C})$, together with $\nu(\text{C}=\text{O})$ and $\nu(\text{N}-\text{H})$ bands when present (Figure 4). The $\nu(\text{RuC}\equiv\text{C})$ metal-coordinated alkynyl bands were present between 2054 and 2066 cm⁻¹ for all complexes in the closed-shell, 18e configuration, while the 17e Ru alkynyl complexes derived by oxidation were characterized by the appearance of a broad and asymmetric $\nu(\text{RuC}\equiv\text{C})$ band at 1900 cm⁻¹.^{38,45,55} The aryl ring breathing mode gains in intensity on oxidation and appears as an intense band between 1568 and 1592 cm⁻¹ for all complexes except 3f, where upon oxidation to [3f]^{•+} the $\nu(\text{C}\equiv\text{C})$ mode decreases in intensity and shifts to lower wavenumbers. The less intense $\nu(\text{C}\equiv\text{C})$ from the noncoordinated C≡C moiety in 3f and 4, present at 2148 cm⁻¹, shifted toward slightly higher wavenumbers (2153 cm⁻¹) and lost intensity on oxidation. Vibrational frequencies computed within the harmonic approach at the optimized structures are fully consistent with the recorded spectra of [3f]ⁿ⁺, [3h]ⁿ⁺, [4]ⁿ⁺, and [5]ⁿ⁺ ($n = 0, 1$; Table 4) (see the Supporting Information) after scaling by an empirical factor of 0.95.^{56,57} The oxidized species [3h]^{•+}, [4]^{•+}, and [5]^{•+} were also characterized by low-intensity bands between 3400 and 3200 cm⁻¹, attributed to the $\nu(\text{N}-\text{H})$ mode. Frequency calculations with computational models of 3h and 4 confirm the extremely weak oscillator strength of the $\nu(\text{N}-\text{H})$ band for these systems (see below). The calculations also predict a marked increase in the intensity of the N-H bands on oxidation, in good agreement with the

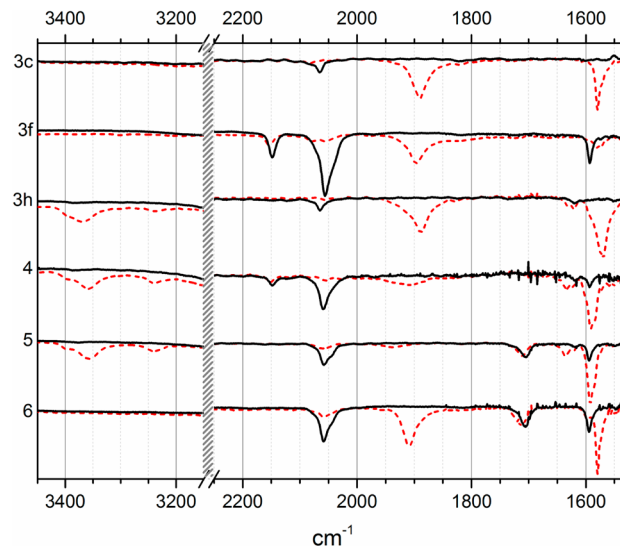


Figure 4. IR spectra of complexes [trans-Ru(C \equiv CC₆H₄R¹-4)(dppe)₂]ⁿ⁺ (R¹ = OMe (3c), C \equiv CSiMe₃ (3f), NH₂ (3h)) and [trans-Ru(C \equiv CC₆H₄R¹-4)(C \equiv CC₆H₄R²-4)(dppe)₂]ⁿ⁺ (R¹ = NH₂, R² = C \equiv CSiMe₃ (4); R¹ = NH₂, R² = CO₂Me (5); R¹ = OMe, R² = CO₂Me (6)): (black solid line) $n = 0$; (red dotted line) $n = 1$.

spectroscopic data recorded. Overall, the IR studies strongly suggest a great degree of ligand redox activity in these complexes.

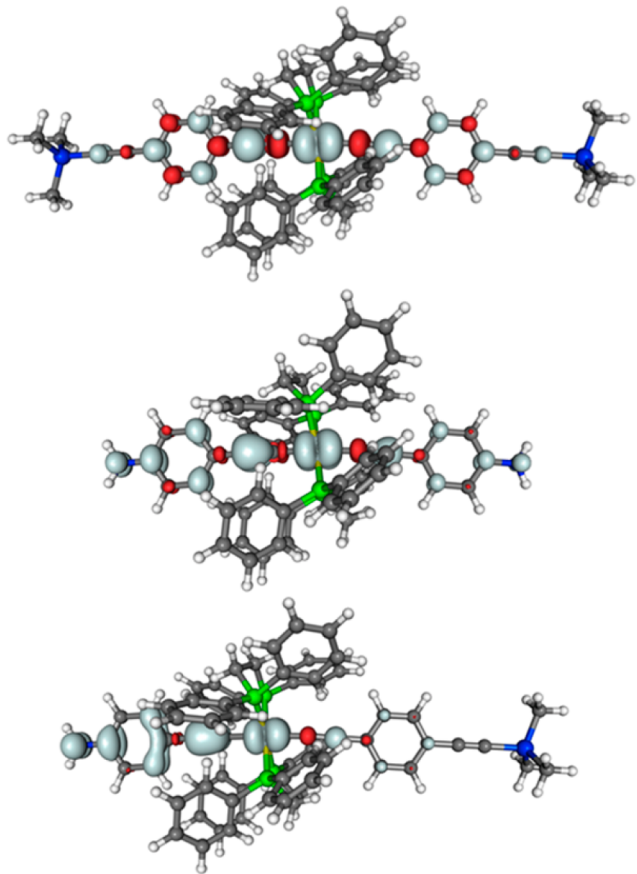
The redox activity of the alkynyl ligands is indicated by the spin densities obtained from the DFT structure optimizations of [3f]^{•+}, [3h]^{•+}, [4]^{•+}, and [5]^{•+} (e.g., Figure 5).⁵⁸ The optimized structures, derived from C₁-symmetric starting geometries, have the ethynyl-aromatic moiety bisecting the dppe ligands and are now defined here as *in-plane*-[3f]^{•+}, *in-plane*-[3h]^{•+}, *in-plane*-[4]^{•+}, and *in-plane*-[5]^{•+}. However, while the Ru(dppe)₂ fragment contributes significantly in all cases (*in-plane* structures: [3f]^{•+}, 71%; [3h]^{•+}, 54%; [4]^{•+}, 43%; [5]^{•+}, 57%), the ligand involvement depends strongly on the substitution of the aromatic unit, and for *in-plane*-[3f]^{•+} the outermost parts of the alkynyl ligands barely contribute (4-Me₃SiC \equiv CC₆H₄/C \equiv C/Ru(dppe)₂/C \equiv C/C₆H₄C \equiv CSiMe₃-4: 7%/11%/71%/6%/5%) (Figure 5). Thus, while the spin density is high on the C \equiv CC₆H₄NH₂-4 ligands in *in-plane*-[4]^{•+} (57%) and *in-plane*-[5]^{•+} (40%), the alkyne ligand bearing the less electron donating substituent is largely innocent (*in-plane*-[4]^{•+}, C \equiv CC₆H₄C \equiv CSiMe₃-4 3%; *in-plane*-[5]^{•+}, C \equiv CC₆H₄CO₂Me-4 7%). It is also noteworthy that for *in-plane*-[3h]^{•+} the spin density is partially localized on one ligand and the ruthenium unit but little on the other alkynyl ligand. The DFT calculations therefore suggest that, at least in these conformations, the complexes *in-plane*-[3h]^{•+}, *in-plane*-[4]^{•+} and *in-plane*-[5]^{•+} might be considered as further examples of metal-bridged organic mixed-valence systems.^{59,60}

With this notion of metal-bridged, organic mixed-valence character in mind, the observation of the low-energy tail of a NIR electronic transition band in the IR spectra of [3h]^{•+} and [4]^{•+} between 7000 and 5500 cm⁻¹ is intriguing, with similar low-energy bands having been observed in closely related complexes by Rigaut, Winter, and colleagues,^{38,45} prompting further consideration of the underlying electronic transitions here.

A series of UV-vis/NIR spectroelectrochemical experiments (Figure 6), supported by time-dependent DFT (TDDFT)

Table 4. Experimental and Calculated (Italic Entries) Vibrational Frequencies of $[3f]^{•+}$, $[3h]^{•+}$, $[4]^{•+}$, and $[5]^{•+}$

Complex	$\nu(\text{Ru}-\text{C}\equiv\text{C})$	$\nu(\text{C}=\text{C}_{\text{aryl}})$	$\nu(\text{C}\equiv\text{C})$	$\nu(\text{N}-\text{H})$	$\nu(\text{C}=\text{O})$
$[3f]^{•+}$	1899 (m)	1580 (w)	2155 (w)		
	1981 (s)	1484 (w)	2180 (w), 2177 (w), 2034 (w)		
$[3h]^{•+}$	1890 (s)	1574 (s)		3370 (m), 3235 (w)	
	1942 (s)	1583 (m), 1581 (m), 1578 (m)		3458 (w), 3446 (w)	
$[4]^{•+}$	1912 (m)	1592 (s)	2153 (w)	3360 (m), 3235 (w)	
	1964 (m)	1587 (s), 1582 (w)	2179 (w), 2078 (w)	3460 (w)	
$[5]^{•+}$	1933 (w)	1593 (s)		3361 (m), 3242 (w)	1712 (m)
	1934 (s)	1576 (s), 1559 (m)		3464 (m)	1735 (w)

Figure 5. Spin-density isosurface plots (± 0.002 au) of $[3f]^{•+}$, $[3h]^{•+}$, and $[4]^{•+}$ (top to bottom) calculated at the BLYP35/COSMO- (CH_2Cl_2) level.

studies, was performed on **3f,h**, **4**, and **5** as representative examples. For **3f,h**, **4**, and **5** a well-defined UV absorption band was observed for each in the electronic spectrum, at 26667 cm^{-1} (**3f**), 31847 cm^{-1} (**3h**), 26316 cm^{-1} (**4**), and 25839 cm^{-1} (**5**), respectively (Figure 6). Upon oxidation in the OTTLE cell, the main absorption band of four complexes undergoes a marked intensity loss and several new features develop in the NIR region of the spectra (Table 5).

Turning attention initially to the symmetrically substituted complexes, Gaussian09 TDDFT calculations at the fully optimized structures give only one intense ($\mu_{\text{trans}} > 1.0$ D) transition below 15000 cm^{-1} : at 11316 cm^{-1} ($\mu_{\text{trans}} = 9.7$ D) for *in-plane*- $[3f]^{•+}$ and at 7778 cm^{-1} ($\mu_{\text{trans}} = 11.7$ D) for *in-plane*- $[3h]^{•+}$, arising in each case from the β -HOMO– β -SOMO excitation (Table 6). While for both complexes the β -HOMO features significant contributions from both alkynyl ligands (contribution from $4-\text{RC}_6\text{H}_4\text{C}\equiv\text{C}/\text{C}\equiv\text{CC}_6\text{H}_4\text{R}-4$ for *in-plane*-

$[3f]^{•+}$ 44%/41% and for *in-plane*- $[3h]^{•+}$ 37%/54%) with the $\text{Ru}(\text{dppe})_2$ unit barely contributing (*in-plane*- $[3f]^{•+}$ 8%; *in-plane*- $[3h]^{•+}$ 4%), the β -SOMO is mainly $\text{C}\equiv\text{CRu}(\text{dppe})_2\text{C}\equiv\text{C}$ centered for *in-plane*- $[3f]^{•+}$ (75%) but is localized at one $\text{C}\equiv\text{CC}_6\text{H}_4\text{NH}_2-4$ ligand (40%) and the $\text{Ru}(\text{dppe})_2$ moiety (39%) for *in-plane*- $[3h]^{•+}$. Hence, the main NIR transition in both symmetrical complexes *in-plane*- $[3f]^{•+}$ and *in-plane*- $[3h]^{•+}$ has appreciable ligand–metal CT (LMCT) character, which is more pronounced for *in-plane*- $[3f]^{•+}$, and is blended with some interligand IVCT (or $\text{L}(\text{L}^+) \text{CT}$) character in the case of *in-plane*- $[3h]^{•+}$.

In addition to the main NIR transitions at 8333 cm^{-1} , the spectrum of $[3f]^{•+}$ features similar shoulders at 9328 and 10417 cm^{-1} , while $[3h]^{•+}$ exhibits an intense shoulder with a band center at 10822 cm^{-1} in addition to the main absorption at 7662 cm^{-1} . Recently the appearance of such shoulders on NIR (and IR) bands in mixed-valence complexes was assigned on the basis of quantum-chemical calculations to the presence of different thermally accessible conformational structures,^{61–63} and synthetic restriction to a small conformational subspace led to an appreciable decrease of intensity of the shoulder in experiments.⁶⁴ Different configurations of the $\text{C}\equiv\text{CC}_6\text{H}_4\text{R}-4$ ligands found in the crystal structures (Table 2) point toward a conformational distribution in solution being a possible explanation for these additional spectral features (vide infra).

TDDFT calculations on the *in-plane* conformation of the unsymmetrically substituted complexes $[4]^{•+}$ and $[5]^{•+}$ gave each one intense transition below 15000 cm^{-1} . For *in-plane*- $[4]^{•+}$ the computed β -HOMO– β -SOMO excitation (8999 cm^{-1} , $\mu_{\text{trans}} = 11.2$ D) is in good agreement with the experimentally obtained band at 9191 cm^{-1} (Table 6). Analogously to *in-plane*- $[3f]^{•+}$ and *in-plane*- $[3h]^{•+}$, the β -HOMO of *in-plane*- $[4]^{•+}$ is effectively delocalized over the molecular backbone ($4-\text{NH}_2\text{C}_6\text{H}_4/\text{C}\equiv\text{CRu}(\text{dppe})_2\text{C}\equiv\text{C}/\text{C}_6\text{H}_4\text{C}\equiv\text{CSiMe}_3-4$ 24%/46%/20%), while the β -SOMO is essentially localized on the $4-\text{NH}_2\text{C}_6\text{H}_4\text{C}\equiv\text{C}$ ligand (60%) and the $\text{Ru}(\text{dppe})_2$ moiety (29%) and the $\text{C}\equiv\text{CC}_6\text{H}_4\text{C}\equiv\text{CSiMe}_3-4$ ligand barely contributes (5%) (Table 6). This principal contribution to the NIR spectrum can therefore be approximated better as an IVCT (interligand, $\text{L}(\text{L}^+) \text{CT}$) transition between the arylacetylidyl ligand moieties linked by the *trans*-{ $\text{Ru}(\text{dppe})_2$ } bridge with even more IVCT character than in *in-plane*- $[3h]^{•+}$ and not as an LMCT transition, as proposed for the symmetrically substituted complex *in-plane*- $[3f]^{•+}$. However, once again a high-energy shoulder at 11507 cm^{-1} and a low-energy feature with low intensity are observed in the recorded spectrum, which cannot be explained by TDDFT calculations on the basis of only the lowest energy conformation. For *in-plane*- $[5]^{•+}$ the β -HOMO– β -SOMO transition at 9286 cm^{-1} ($\mu_{\text{trans}} = 11.1$ D) is also the only excitation for which appreciable intensity is computed, and it is

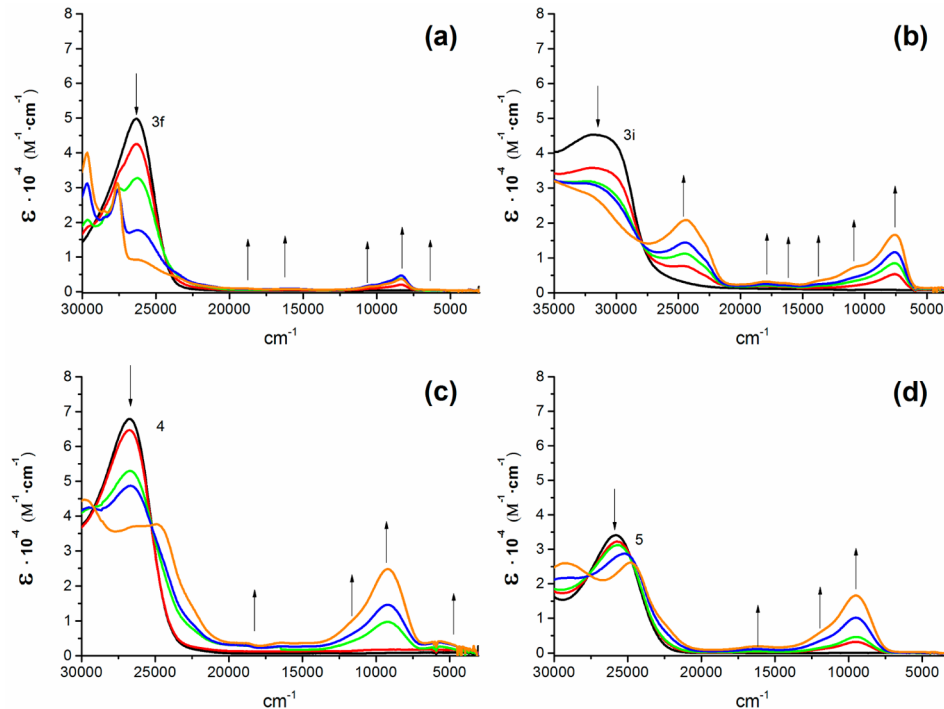


Figure 6. UV/vis/NIR spectral changes of (a) 3f, (b) 3h, (c) 4, and (d) 5 during the first oxidation process.

Table 5. UV/Vis/NIR Spectral Data of [3f]•+, [3h]•+, [4]•+, and [5]•+ Obtained upon Oxidation of 3i,f, 4, and 5

complex	$\nu_{\max}/\text{cm}^{-1}$ [$\epsilon/10^4 \text{ M}^{-1} \text{ cm}^{-1}$]
[3f]•+	23640 [0.4], 18761 [0.1], 15625 [0.1], 10417 [0.2], 9328 [0.3], 8333 [0.5], 6131 [0.1]
[3h]•+	24331 [2.1], 22779 [1.4], 18214 [0.3], 16339 [0.3], 13679 [0.3], 10822 [0.7], 7662 [1.6]
[4]•+	24814 [3.7], 22522 [1.4], 18727 [0.4], 16474 [0.4], 11507 [1.0], 9191 [2.5], 5695 [0.4]
[5]•+	24691 [2.6], 22573 [0.9], 16155 [0.2], 12062 [0.6], 9551 [1.6]

of similar mixed LMCT and interligand IVCT character as the transition calculated for *in-plane*-[3h]•+.

As the UV/vis/NIR band envelopes of [3f]•+, [3h]•+, [4]•+, and [5]•+ cannot be explained by a single minimum energy conformation, the influence of different conformational forms on the appearance of the UV/vis/NIR spectrum was investigated quantum chemically (Table 6) using [3h]•+ by way of example. The influence of the orientation of the aryl portion of the C≡CC₆H₄NH₂-4 ligand relative to the ruthenium moiety in [3h]•+ was examined by varying the previously described torsion angle θ in a range from 0 to 90° (Figure 3). Additionally, the conformation of the two C≡CC₆H₄NH₂-4 aryl moieties relative to each other was explored by varying the torsion angle Ω from 0 to 90° (Figure 7; see Computational Details). The resulting potential-energy surface (PES) is shown in the Supporting Information. The minimum on the PES is found for the conformation $\theta \approx 0^\circ$, $\Omega = 20^\circ$, and the maximum ($\theta \approx 90^\circ$, $\Omega = 30^\circ$) is computed to be only 16.6 kJ/mol higher in energy.

The low energy penalty associated with interchanging the lowest- and highest-energy conformations of the two C≡CC₆H₄NH₂-4 ligands for [3h]•+ helps to account for the spectroscopic observations. When Ω is varied with one ligand being fixed at $\theta \approx 0^\circ$, the rotational barrier is only 3.2 kJ/mol between the minimum structure at $\Omega = 20^\circ$ and the maximum

at $\Omega = 60^\circ$. As the spin density obtained from the full optimization (see Figure 5) already exhibits slight symmetry breaking, this low barrier can be explained by the tendency of [3h]•+ toward charge localization onto one C≡CC₆H₄NH₂-4 ligand and the metal center. Hence, the C≡CC₆H₄NH₂-4 unit not involved in the charge delocalization can rotate almost freely (Figure 8).

As Ω goes to 90°, the spin density becomes steadily more localized onto one ligand and the ruthenium center, resulting in a clearly symmetry-broken structure for $\Omega = 90^\circ$, which is only 2.5 kJ/mol higher in energy than the minimum. For this structure the frontier orbitals are centered on the Ru(dppe)₂ unit and one ligand (Figure 9). In this conformation, the main electronic excitations at 9900 cm⁻¹ ($\mu_{\text{trans}} = 10.0$ D) arise from the β -HOMO-1– β -SOMO transition. Both of these orbitals are located at the same aniline unit, the phenyl plane of which bisects the dppe ligands (β -HOMO-1, 42%; β -SOMO, 24%) and the C≡CRu(dppe)₂C≡C unit (β -HOMO-1, 49%; β -SOMO, 70%). They are of π and π^* character, respectively. Thus, only a small amount of charge is transferred upon excitation. Obviously, although the experimental excitation energy of 10822 cm⁻¹ is underestimated, this transition can be assigned to the high-energy shoulder obtained in the UV/vis/NIR spectrum.

The rotation of both C≡CC₆H₄NH₂-4 ligands out of the plane bisecting the dppe ligands when θ is increased from 0°, while the relative conformation of the ligands is kept at $\Omega = 0^\circ$, is associated with a barrier more sizable than that for the rotation of only one ligand (vide supra). A minimum at $\theta \approx 90^\circ$, which is disfavored by only 3.2 kJ/mol in comparison to the minimum of the relaxed scan and by 2.6 kJ/mol in comparison to the lowest-energy structure at $\theta \approx 0^\circ$ of the PES cut at $\Omega = 0^\circ$ also likely contributes to the overall spectral profile. TDDFT calculations using this local minimum ($\theta \approx 90^\circ$, $\Omega = 0^\circ$) give two excitations below 15000 cm⁻¹ with $\mu_{\text{trans}} > 1.0$ D. The more intense excitation at 7849 cm⁻¹ ($\mu_{\text{trans}} =$

Table 6. Representations of the Molecular Conformations (θ and Ω in deg) of the Key Structures on the PES of Compounds $[3f]^{*+}$, $[3h]^{*+}$, $[4]^{*+}$, and $[5]^{*+}$, Summary of the Main TDDFT Excitations, and Contributions to the Involved β Orbitals

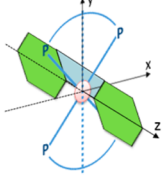
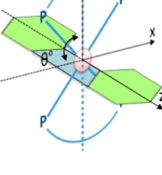
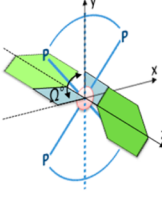
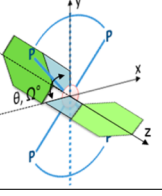
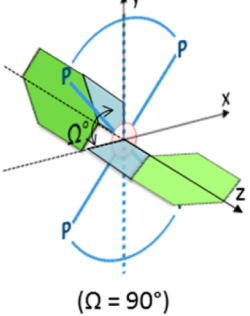
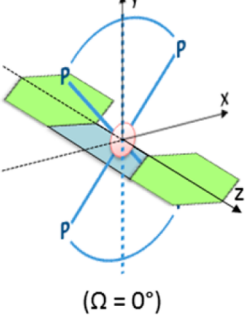
Conformer	Angles [°]	Complex	Main calculated transition [cm ⁻¹] (μ_{trans} [D])	Orbitals	Contributions [%]				
					R ¹ C ₆ H ₄	C≡C	[Ru]	C≡C	C ₆ H ₄ R ²
	$\theta = 0$ $\Omega = 0$	<i>In-plane-</i> $[3f]^{*+}$	11316 (9.7)	β -SOMO	11	15	50	10	8
			7778 (11.7)	β -HOMO	25	19	8	18	23
			8999 (11.2)	β -SOMO	(NH ₂) 31	29	29	4	1
			9286 (11.1)	β -HOMO	(NH ₂) 24	7	17	22	20
			9286 (11.1)	β -SOMO	(NH ₂) 23	22	39	6	4
	$\theta = 90$ $\Omega = 0$	<i>In-plane-</i> $[3h]^{*+}$	one negative exc.	β -SOMO	0	15	65	12	0
			8268 (11.6)	β -HOMO	27	21	18	13	15
			9198 (11.1)	β -SOMO	(NH ₂) 36	31	23	3	0
			9024 (11.6)	β -HOMO	(NH ₂) 18	5	13	27	29
			9024 (11.6)	β -SOMO	(NH ₂) 31	26	30	5	1
	$\theta = 0$ $\Omega = 90$	<i>perp-</i> $[3f]^{*+}$	12287 (8.1)	β -SOMO	13	18	54	9	0
			9295 (10.7)	β -HOMO- ₁	0	7	19	28	41
			9555 (10.2)	β -SOMO	(NH ₂) 33	30	29	4	0
			9709 (10.4)	β -HOMO- ₁	(NH ₂) 36	7	31	18	0
			9709 (10.4)	β -SOMO	(NH ₂) 28	27	35	5	0
	$\theta = 90$ $\Omega = 90$	<i>perp-</i> $[3h]^{*+}$	10072 (10.0)	β -SOMO	(NH ₂) 38	32	23	3	0
			9381 (9.9)	β -HOMO- ₁	(NH ₂) 31	6	31	23	0
			9381 (9.9)	β -SOMO	(NH ₂) 0	12	57	15	9
			9381 (9.9)	β -HOMO- ₁	0	19	19	26	19
	$\theta = 90$ $\Omega = 90$	<i>perp-</i> $[4]^{*+}$							
	$\theta = 90$ $\Omega = 0$	<i>perp-</i> $[5]^{*+}$							

Figure 7. Representation of angle Ω in *trans*-Ru(\equiv CC₆H₄R¹)₂(dppe)₂.

12.1 D) arises from the β -HOMO– β -SOMO transition and appears at very similar energy as for *in-plane*- $[3h]^{*+}$. Indeed, the orbital distribution is comparable to that for the fully optimized structure (4-RC₆H₄C≡C/Ru(dppe)₂/C≡CC₆H₄R-4: β -HOMO, 34%/2%/58%; β -SOMO, 45%/34%/17%) (Figure 10), but the orbitals offer a series of nodal planes perpendicular to those described for the fully optimized structure (Figure 10).

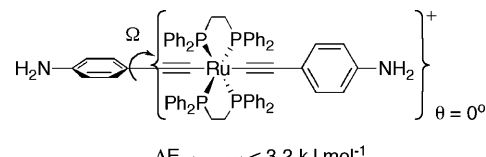


Figure 8. Rotational barrier for $[3h]^{*+}$ with $\theta = 0^\circ$.

At 11959 cm⁻¹ ($\mu_{\text{trans}} = 1.5$ D) a second, less intense excitation arises from the β -HOMO-5 to the β -SOMO, corresponding to a metal–ligand CT (the β -HOMO-5 exhibits almost exclusively metal character, 83%).

To perform vibrational analyses within the harmonic framework, selected points on the PES were reoptimized without constraints. The minima, indicated by the absence of imaginary frequencies, gave computed frequencies very similar to that for the lowest energy structure *in-plane*- $[3h]^{*+}$ ($\nu(\text{RuC}\equiv\text{C})$ 1942 cm⁻¹). Optimizations starting from the two points $[3h]^{*+}$ ($\theta \approx 0^\circ$, $\Omega = 90^\circ$) and $[3h]^{*+}$ ($\theta \approx 90^\circ$, $\Omega = 0^\circ$) gave the two minima *perp*- $[3h]^{*+}$ and *out-of-plane*- $[3h]^{*+}$. TDDFT calculations give the same main spectral features for the minima *perp*- $[3h]^{*+}$ at 8268 cm⁻¹ ($\mu_{\text{trans}} = 11.6$ D) and for

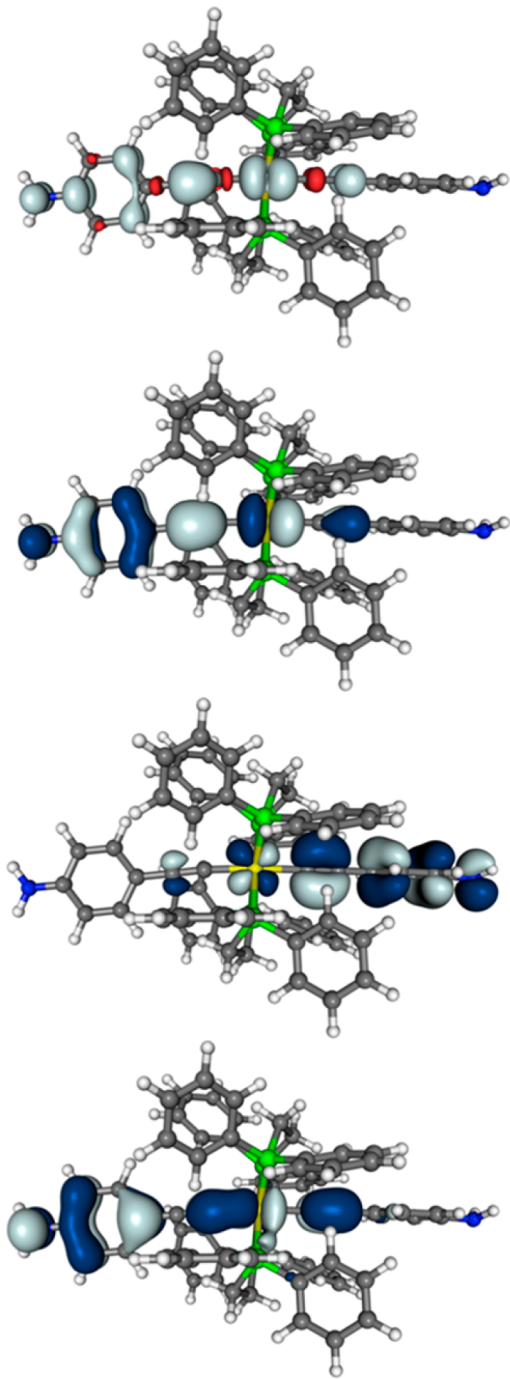


Figure 9. Isosurface plots of the spin density (± 0.002 au, top) and the β frontier orbitals (± 0.03 au) β -SOMO, β -HOMO, and β -HOMO-1 of $[3h]^{•+}$ with one $C\equiv CC_6H_4NH_2-4$ ligand in plane and one perpendicular to the other (second from top to bottom) ($\theta \approx 0^\circ, \Omega = 90^\circ$) calculated at the BLYP35/COSMO(CH_2Cl_2) level.

out-of-plane-[3h] $^{•+}$ at 9295 cm^{-1} ($\mu_{trans} = 10.7\text{ D}$), as observed for the corresponding relaxed-scan structures (Table 6). In addition, the previously discussed low-intensity MLCT excitations are computed at 11558 cm^{-1} ($\mu_{trans} = 1.2\text{ D}$) and 11526 cm^{-1} ($\mu_{trans} = 1.3\text{ D}$). However, fully optimized structures *perp-[3h] $^{•+}$* and *out-of-plane-[3h] $^{•+}$* are slightly favored energetically (by 2.7 and 2.0 kJ/mol, respectively). Hence, within the accuracy of the method all three structures are more or less isoenergetic and all would contribute significantly to the observed spectroscopic profile. Vibrational

analysis gave $\nu(RuC\equiv C)$ at 1930 cm^{-1} for *perp-[3h] $^{•+}$* and 1915 cm^{-1} for *out-of-plane-[3h] $^{•+}$* , which is in good agreement with the slightly broadened $\nu(RuC\equiv C)$ peak found experimentally for $[3h]^{•+}$ (Figure 4). Hence, the finding of different rotameric forms contributing to the UV-vis/NIR spectrum is fully consistent with the experimentally observed IR signature.

Extending this method of analysis to complexes $[3f]^{•+}$, $[4]^{•+}$, and $[5]^{•+}$ and starting from inputs, in which one ($\theta \approx 0^\circ, \Omega = 90^\circ$) or both ligands ($\theta \approx 90^\circ, \Omega = 0^\circ$) are perpendicular to the plane bisecting the dppe ligands, we optimized structures without constraints (Table 6). For $[4]^{•+}$ and $[5]^{•+}$, the $C\equiv CC_6H_4NH_2-4$ and the $C\equiv CC_6H_4C\equiv CSiMe_3-4$ or $C\equiv CC_6H_4CO_2Me-4$ ligands, respectively, were investigated in perpendicular positions with the other corresponding ligand in the plane bisecting the dppe ligands. For *perp-[3f] $^{•+}$* , which is disfavored by only 1.9 kJ/mol in comparison to the minimum at $\theta \approx 0^\circ, \Omega \approx 0^\circ$, the only electronic transition found below 15000 cm^{-1} is at 12287 cm^{-1} ($\mu_{trans} = 8.1\text{ D}$). This is blue-shifted by about 1000 cm^{-1} in comparison to that for *in-plane-[3f] $^{•+}$* ($\theta \approx 0^\circ, \Omega \approx 0^\circ$). Analogously to $[3h]^{•+}$, the main difference in the spectroscopic properties of the various minima is seen in the orbital contributions. The excitation of *perp-[3f] $^{•+}$* arises from the β -HOMO-1– β -SOMO transition. Both orbitals are localized at one $C_6H_4C\equiv CSiMe_3-4$ and the $C\equiv CRu(dppe)_2C\equiv C$ unit with the other $C_6H_4C\equiv CSiMe_3-4$ not contributing (0% for both orbitals) (Table 6). *out-of-plane-[3f] $^{•+}$* , the structure with both ligands rotated out of plane, is 11.3 kJ/mol higher in energy, and thus its contribution to the spectrum is only minor (the TDDFT calculations gave one negative excitation energy for this structure). Both *in-plane-[3f] $^{•+}$* and *perp-[3f] $^{•+}$* exhibit an additional low-intensity transition ($\mu_{trans} < 0.5\text{ D}$) at 8825 and 8517 cm^{-1} , respectively, arising from metal-centered orbitals. These excitations may exhibit or even gain intensity for other rotameric forms, and thus they may offer a possible explanation for the weak lowest-energy band in the experimental spectrum (Tables 5 and 6).

As expected for $[4]^{•+}$ and $[5]^{•+}$, the structures with $\theta \approx 0^\circ, \Omega \approx 90^\circ$ exhibit spectral features similar to those for the minimum energy structure (Table 6). For these two examples we define θ as the angle between the $C\equiv CC_6H_4NH_2-4$ ligand and the plane bisecting the dppe ligands, noting that the ligands $C\equiv CC_6H_4C\equiv CSiMe_3-4$ in $[4]^{•+}$ and $C\equiv CC_6H_4CO_2Me-4$ in $[5]^{•+}$ are perpendicular to the plane bisecting the dppe ligands for $\theta \approx 0^\circ, \Omega \approx 90^\circ$. TDDFT yields an intense β -HOMO-1– β -SOMO excitation at 9555 cm^{-1} ($\mu_{trans} = 10.2\text{ D}$) for $[4]^{•+}$ and at 9709 cm^{-1} ($\mu_{trans} = 10.2\text{ D}$) for $[5]^{•+}$. While the contributions to the β -SOMO stay nearly unchanged in comparison to the minimum structures (see the Supporting Information), the β -HOMO-1 is localized on the $C_6H_4NH_2-4$ ligand ($[4]^{•+}, 36\%$; $[5]^{•+}, 38\%$) and the $C\equiv CRu(dppe)_2C\equiv C$ unit ($[4]^{•+}, 56\%$; ($[5]^{•+}, 53\%$).

For the structure of $[4]^{•+}$ with $\theta \approx 90^\circ, \Omega \approx 90^\circ$ in which the $C\equiv CC_6H_4NH_2-4$ ligand is perpendicular to the plane bisecting the dppe ligands, the dominant feature is again the β -HOMO-1– β -SOMO transition ($10072\text{ cm}^{-1}, \mu_{trans} = 10.0\text{ D}$). This excitation exhibits ligand $\pi-\pi^*$ character accompanied by small LMCT contributions and is probably responsible for the high-energy shoulder observed in the experimental spectrum (Figure 6). A second low-intensity excitation from the lower-lying orbitals β -HOMO-5 and β -HOMO-4, which are metal-centered, to the β -SOMO is computed at 13613 cm^{-1} ($\mu_{trans} = 1.2\text{ D}$). For $[5]^{•+}$ this structure likely makes only a relatively

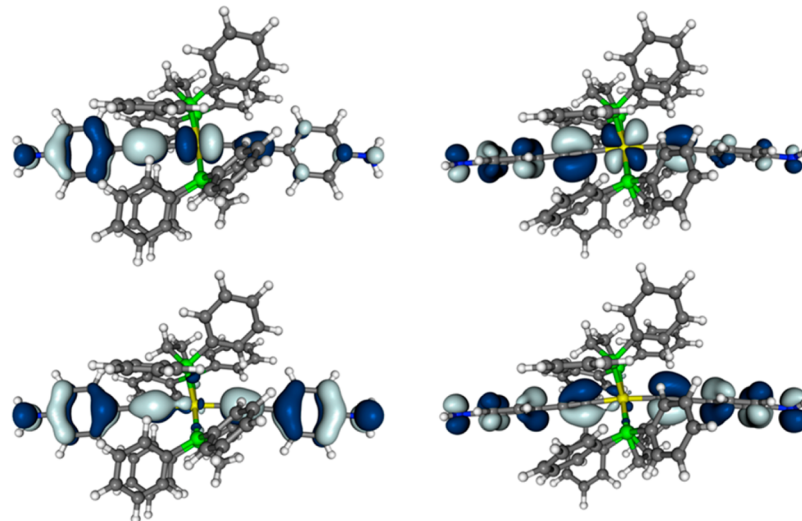


Figure 10. Isosurface plots (± 0.03 au) of the β -SOMO (top) and the β -HOMO (bottom) for *in-plane*- $[3h]^{•+}$ (left) and for the structure at $\theta \approx 90^\circ, \Omega = 0^\circ$ of $[3h]^{•+}$ (right; both aromatic rings of the ligand are perpendicular to the plane bisecting the dppe ligands) calculated at the BLYP35/COSMO(CH_2Cl_2) level.

minor contribution to the UV-vis/NIR spectrum, as it is disfavored by 16.4 kJ/mol.

Again, for both asymmetric complexes the computed excitations for the *out-of-plane* structures ($\theta \approx 90^\circ, \Omega \approx 0^\circ$) are very similar to those of the *in-plane* structures (Table 6). The β -HOMO– β -SOMO transition appears slightly blue-shifted at 9198 cm^{-1} ($\mu_{\text{trans}} = 11.1\text{ D}$) for *out-of-plane*- $[4]^{•+}$ and slightly red-shifted at 9024 cm^{-1} ($\mu_{\text{trans}} = 11.6\text{ D}$) for *out-of-plane*- $[5]^{•+}$. For *out-of-plane*- $[4]^{•+}$ the previously discussed low-intensity LMCT excitation from the lower-lying orbitals β -HOMO-5 and β -HOMO-4 is also found at 13461 cm^{-1} ($\mu_{\text{trans}} = 1.0\text{ D}$). Again, low-intensity transitions of mixed LMCT/IVCT character are found for the different conformers of $[4]^{•+}$ between 3740 cm^{-1} ($\mu_{\text{trans}} = 0.9\text{ D}, \theta \approx 90^\circ, \Omega \approx 90^\circ$) and 5037 cm^{-1} ($\mu_{\text{trans}} = 0.1\text{ D}$, *in-plane*- $[4]^{•+}$), which may explain the lowest energy absorption band in the experimental spectrum (Tables 5 and 6).

CONCLUSIONS

The trans effects of alkynyl ligands bearing substituents R^1 on the reactions of $\text{trans-RuCl}(\text{C}\equiv\text{CC}_6\text{H}_4\text{R}^1\text{-}4)(\text{dppe})_2$ with terminal alkynes were examined. While strongly electron-donating R^1 groups (e.g., NH_2, OMe) stabilize the trans chloride ligand sufficiently to promote the slow formation of bis(alkynyl) complexes, precursors bearing more modestly donating groups ($R^1 = \text{Me}$) or withdrawing groups ($R^1 = \text{NO}_2, \text{CO}_2\text{Me}$) are largely inert to further reaction in the absence of a suitable halide abstracting agent. In the presence of Tl^+ salts and the noncoordinating base DBU, conversion of mono(alkynyl) complexes to symmetrically or unsymmetrically substituted bis(alkynyl) complexes can be achieved in high yields in a matter of minutes as pure precipitates which can be isolated from the reaction mixtures by simple filtration. These complexes undergo one or more electrochemical oxidations, which are shown by IR spectroelectrochemical methods to be substantially alkynyl ligand in character.

Quantum-chemical calculations at the DFT and TDDFT levels on the monooxidized complexes using the BLYP35 functional and continuum solvent models indicate (a) substantial delocalization of spin density between metal centers

and the acetylidy ligand framework, (b) ligand-based mixed-valence character in some of the symmetrical diacetylidy complexes, and (c) substantial importance of the relative conformational arrangement of the aromatic rings of the acetylidy ligands for both electronic and vibrational spectra. That is, the PES of the complexes $[\text{trans-Ru}(\text{C}\equiv\text{CC}_6\text{H}_4\text{R}^1\text{-}4)_2(\text{dppe})_2]^{•+}$ feature several conformational minima. These are close in energy with small barriers between them, and many are likely to be thermally populated in solution at room temperature. These conformations offer electronic transitions that differ in energy and character depending on both the conformation and nature of the aryl ligand substituent. In general, the lowest-energy transitions are associated with LMCT (symmetrically substituted complexes such as $[3f]^{•+}$) or interaryl ligand IVCT (complexes with redox active ligands such as $[3h]^{•+}$ and related asymmetric complexes $[4]^{•+}$ and $[5]^{•+}$) character. The higher-energy shoulders observed in the experimental spectra arise from the slightly higher energy conformations in which one or more of the arylalkynyl moieties has partially lost conjugation with the other side of the complex. The excitations of these conformers have more MLCT and ligand $\pi-\pi^*$ character. These studies have shown that the NIR absorption band envelopes observed for symmetrically and unsymmetrically substituted complexes $[\text{trans-Ru}(\text{C}\equiv\text{CC}_6\text{H}_4\text{R}^1\text{-}4)_2(\text{dppe})_2]^{•+}$ are not accurately described in terms of transitions of one specific character (MLCT, LMCT, IVCT, etc.). Rather, the conformational ensembles present in solution mean that these complex band envelopes arise from transitions with distinct electronic origin, a finding that should be of importance in interpreting the optical and electronic behavior of compounds and materials based on this motif.

EXPERIMENTAL SECTION

General Conditions. All reactions were carried out under an atmosphere of nitrogen, using standard Schlenk techniques. The reaction solvent CHCl_3 was purified and dried using an Innovative Technology SPS-400 system and degassed before use. No special precautions were taken to exclude air during the workup. The metallic salts $[\text{RuCl}(\text{dppe})_2]\text{OTf}$ ([1]OTf)¹⁷ and TIBF_4^{65} were prepared by literature methods. *Warning!* TIBF_4 should always be handled in a well-

ventilated fumehood, and personal protective equipment should be worn throughout. The ligands were synthesized following variations of known preparations when not commercially available (Supporting Information). Compounds **2a–c** were prepared by literature methods.¹⁷ Other compounds were purchased and used as received. Cyclic voltammograms were recorded at $v = 100\text{--}800 \text{ mV s}^{-1}$ from approximately 10^{-4} M solutions in analyte in CH_2Cl_2 with 10^{-1} M NBu_4BF_4 , using a gastight single-compartment three-electrode cell fitted with a platinum-disk working electrode and platinum-wire auxiliary and pseudo reference electrodes. The working electrode surface was polished before scans with alumina paste. The cell was managed by a computer-controlled Autolab PGSTAT-30 potentiostat. IR and UV/vis/NIR spectroelectrochemical experiments were carried out in a CH_2Cl_2 solution of NBu_4BF_4 (0.1 M) using an OTTLE cell⁶⁶ powered by an EmStat2 potentiostat. IR spectra were recorded using a Nicolet Thermo FT6700 or Nicolet Avatar spectrometer, from CH_2Cl_2 solutions or Nujol mulls on CaF_2 plates. UV/vis/NIR spectra were recorded using a Cary 5000 spectrometer from CH_2Cl_2 solutions. NMR spectra were recorded on a 400 MHz Bruker Avance spectrometer from deuterated chloroform solutions. ^1H (400 MHz) and $^{31}\text{P}\{\text{H}\}$ NMR spectra (162 MHz) were referenced against solvent resonances or external H_3PO_4 .

Synthesis of trans-RuCl(C≡CC₆H₄R-4)(dppe)₂ (2d–g). To a solution of $[\text{RuCl}(\text{dppe})_2]\text{OTf}$ ([1]OTf; 0.100 g, 0.092 mmol) and DBU (excess) in CH_2Cl_2 (4 mL) was added the appropriate alkyne (0.10 mmol). The red solution typically turned yellow (with the exception of **2e**) after stirring at room temperature for 1 h. The final products were obtained from the reaction mixture after the appropriate purification (see below).

trans-RuCl(C≡CC₆H₄CO₂Me-4)(dppe)₂ (2d).¹⁷ The yellow solution was filtered through neutral alumina (Brockmann I). Addition of hexane to the filtrate yielded a pale yellow precipitate that was collected by filtration, washed with hexane, and dried in air (97 mg, 97%). ^1H NMR: δ 7.76 (d, $J = 8 \text{ Hz}$, 2H, o-Ph-CO₂Me), 7.45–7.39 (m, 8H, o-PPh₂), 7.36–7.30 (m, 8H, o-PPh₂), 7.23–7.14 (m, 8H, p-PPh₂), 7.05–6.98 (m, 8H, m-PPh₂), 6.98–6.90 (m, 8H, m-PPh₂), 6.57 (d, $J = 8 \text{ Hz}$, 2H, m-Ph-CO₂Me), 3.89 (s, 3H, COO-Me), 2.77–2.59 (m, 8H, dppe). $^{31}\text{P}\{\text{H}\}$ NMR: δ 48.2 (s, dppe). IR (Nujol, cm^{-1}): 2064 (m) ν (Ru—C≡C); 1716 (m) ν (C=O).

trans-RuCl(C≡CC₆H₄NO₂-4)(dppe)₂ (2e).¹⁷ The bright orange solution was filtered through neutral alumina (Brockmann I). Addition of hexane to the filtrate yielded an orange precipitate that was collected by filtration, washed with MeOH, and dried in air (93 mg, 94%). ^1H NMR: δ 7.94 (d, $J = 8 \text{ Hz}$, 2H, o-Ph-NO₂), 7.41–7.30 (m, 16H, o-PPh₂), 7.24–7.17 (m, 8H, p-PPh₂), 7.06–6.99 (m, 8H, m-PPh₂), 6.98–6.91 (m, 8H, m-PPh₂), 6.44 (d, $J = 8 \text{ Hz}$, 2H, m-Ph-NO₂), 2.81–2.58 (m, 8H, dppe). $^{31}\text{P}\{\text{H}\}$ NMR: δ 47.7 (s, dppe). IR (Nujol, cm^{-1}): 2052 (m) ν (Ru—C≡C).

trans-RuCl(C≡CC₆H₄C≡SiMe₃-4)(dppe)₂ (2f).^{11,23} The yellow solution was filtered through neutral alumina (Brockmann I). Addition of hexane to the yellow filtrate yielded the pure product as a yellow precipitate (96 mg, 92%). Single crystals suitable for X-ray diffraction were obtained from CH_2Cl_2 /hexane. ^1H NMR: δ 7.44–7.38 (m, 8H, o-PPh₂), 7.37–7.30 (m, 8H, o-PPh₂), 7.23–7.12 (m, 10H, C₂-Ph-C₂/p-PPh₂), 7.05–6.97 (m, 8H, m-PPh₂), 6.95–6.88 (m, 8H, m-PPh₂), 6.49 (d, $J = 8 \text{ Hz}$, 2H, C₂-Ph-C₂), 2.75–2.61 (m, 8H, dppe), 0.26 (s, 9H, SiMe₃). $^{31}\text{P}\{\text{H}\}$ NMR: δ 50.1 (s, dppe). IR (Nujol, cm^{-1}): 2150 (m) ν (C≡C); 2068 (s) ν (Ru—C≡C).

trans-RuCl(C≡CC₆H₄C≡C^tBu-4)(dppe)₂ (2g). The yellow solution was filtered through neutral alumina (Brockmann I). Addition of Et₂O to the yellow filtrate yielded the pure product as a yellow precipitate (74 mg, 72%). Single crystals suitable for X-ray diffraction were obtained from CDCl_3 /Et₂O. ^1H NMR: δ 7.46–7.41 (m, 8H, o-PPh₂), 7.36–7.30 (m, 8H, o-PPh₂), 7.22–7.12 (m, 10H, C₂-Ph-C₂/p-PPh₂), 7.04–6.98 (m, 8H, m-PPh₂), 6.95–6.89 (m, 8H, m-PPh₂), 6.50 (d, $J = 8 \text{ Hz}$, 2H, C₂-Ph-C₂), 1.33 (s, 9H, CMe₃). $^{31}\text{P}\{\text{H}\}$ NMR: δ 49.2 (s, dppe). IR (Nujol, cm^{-1}): 2183 (w) ν (C≡C); 2068 (s) ν (Ru—C≡C).

trans-RuCl(C≡CC₆H₄C≡CH-4)(dppe)₂ (2i).^{24,25} **2f** (50 mg, 0.044 mmol) was reacted with TBAF (1 M in THF, 50 μL , 0.050 mmol) in CH_2Cl_2 at room temperature overnight. The orange solution

was filtered through basic alumina (Brockmann III) and the filtrate taken to dryness to give the pure product as an orange powder (41 mg, 88%). Single crystals suitable for X-ray diffraction were obtained from CH_2Cl_2 /Et₂O. ^1H NMR: δ 7.50–7.42 (m, 8H, o-PPh₂), 7.35–7.28 (m, 8H, o-PPh₂), 7.25–7.14 (m, 10H, C≡C-Ph-C≡C/p-PPh₂), 7.05–6.98 (m, 8H, m-PPh₂), 6.98–6.92 (m, 8H, m-PPh₂), 6.52 (d, $J = 8 \text{ Hz}$, 2H, C≡C-Ph-C≡C), 3.11 (s, 1H, C≡C-H), 2.78–2.59 (m, 8H, dppe). $^{31}\text{P}\{\text{H}\}$ NMR: δ 50.3 (s, dppe). IR (Nujol, cm^{-1}): 3270 (s) ν (C≡C-H); 2050 (m) ν (Ru—C≡C).

Synthesis of trans-Ru(C≡CC₆H₄R-4)₂(dppe)₂ (3a–g). To a solution of $[\text{RuCl}(\text{dppe})_2]\text{OTf}$ ([1]OTf; 0.100 g, 0.092 mmol) and DBU (excess) in CH_2Cl_2 (4 mL) was added a slight excess of the appropriate alkyne (0.20 mmol). The resulting red solution typically turned yellow after stirring at room temperature for 20 min. To the yellow solution was added 1 equiv of TiBF₄ (0.027 g, 0.092 mmol), and the off-white precipitate (TlCl) was carefully removed by filtration. The final products were obtained from the filtrate after the appropriate purification (vide infra).

trans-Ru(C≡CC₆H₄Me-4)₂(dppe)₂ (3a).¹⁵ The TlCl precipitate was removed by filtration through neutral alumina (Brockmann I). Addition of hexane to the yellow filtrate yielded the pure product as a pale yellow precipitate (72 mg, 69%). Single crystals suitable for X-ray diffraction were obtained from hot toluene. ^1H NMR: δ 7.56–7.48 (m, 16H, o-PPh₂), 7.20–7.12 (m, 8H, p-PPh₂), 7.05–6.85 (m, 20H, Ph-Me/o-PPh₂), 6.67 (d, $J = 8 \text{ Hz}$, 4H, Ph-Me), 2.65–2.56 (m, 8H, dppe), 2.31 (s, 6H, OMe). $^{31}\text{P}\{\text{H}\}$ NMR: δ 53.2 (s, dppe). IR (Nujol, cm^{-1}): 2069 (m) ν (Ru—C≡C).

trans-Ru(C≡CC₆H₅H₁₁-4)₂(dppe)₂ (3b). The TlCl precipitate was removed by filtration through neutral alumina (Brockmann I). The pure product precipitated out of the filtrate as pale yellow solids upon addition of MeOH (59 mg, 52%). Crystals suitable for X-ray diffraction were obtained from CHCl_3 /MeOH. ^1H NMR: δ 7.58–7.47 (m, 16H, o-PPh₂), 7.20–7.15 (m, 8H, p-PPh₂), 7.00–6.92 (m, 20H, Ph-C₅H₁₁/m-PPh₂), 6.70 (d, $J = 8 \text{ Hz}$, 4H, Ph-C₅H₁₁), 2.65–2.52 (m, 12H dppe/ α -CH₂), 1.63 (q, $J = 7 \text{ Hz}$, 4H, β -CH₂), 1.40–1.34 (m, 8H, γ,δ -CH₂), 0.93 (t, $J = 7 \text{ Hz}$, 6H, ϵ -CH₂). $^{31}\text{P}\{\text{H}\}$ NMR: δ 55.0 (s, dppe). IR (Nujol, cm^{-1}): 2065 (m) ν (Ru—C≡C). Anal. Calcd: C, 75.46; H, 5.36. Found: C, 75.27; H, 6.08. The discrepancy likely indicates residual chloroform solvate.

trans-Ru(C≡CC₆H₄OMe-4)₂(dppe)₂ (3c). The TlCl precipitate was removed by filtration through neutral alumina (Brockmann I). The pure product was obtained from the filtrate as a yellow precipitate upon addition of Et₂O (67 mg, 63%). Single crystals suitable for X-ray diffraction were obtained from hot toluene. ^1H NMR: δ 7.56–7.50 (m, 16H, o-PPh₂), 7.19–7.12 (m, 8H, p-PPh₂), 6.97–6.91 (m, 16H, m-PPh₂), 6.79 (s, 8H, C₂-Ph-OMe), 3.80 (s, 6H, OMe), 2.65–2.56 (m, 8H, dppe), $^{31}\text{P}\{\text{H}\}$ NMR: δ 54.1 (s, dppe). IR (Nujol, cm^{-1}): 2069 (m) ν (Ru—C≡C). Anal. Calcd: C, 72.46; H, 5.39. Found: C, 72.65; H, 5.38.

trans-Ru(C≡CC₆H₄CO₂Me-4)₂(dppe)₂ (3d). The TlCl precipitate was removed by filtration through neutral alumina (Brockmann I). The pure product precipitated from the filtrate as pale yellow solids upon addition of Et₂O (67 mg, 60%). Crystals suitable for X-ray diffraction were obtained from CH_2Cl_2 /Et₂O. ^1H NMR: δ 7.81 (d, $J = 8 \text{ Hz}$, 4H, o-Ph-CO₂Me), 7.51–7.44 (m, 16H, o-PPh₂), 7.20–7.14 (m, 8H, p-PPh₂), 6.98–6.90 (m, 16H, m-PPh₂), 6.71 (d, $J = 8 \text{ Hz}$, 4H, m-Ph-CO₂Me), 3.90 (s, 6H, COO-Me), 2.68–2.57 (m, 8H, dppe). $^{31}\text{P}\{\text{H}\}$ NMR: δ 54.4 (s, dppe). IR (Nujol, cm^{-1}): 2058 (s) ν (Ru—C≡C); 1722 (m) ν (C=O). Anal. Calcd: C, 71.04; H, 5.13. Found: C, 70.96; H, 4.97.

trans-Ru(C≡CC₆H₄NO₂-4)₂(dppe)₂ (3e).¹⁵ The TlCl precipitate was removed from the red mixture upon filtration through neutral alumina (Brockmann I). The red solids that precipitated from the filtrate upon addition of Et₂O were collected by filtration and purified further by preparatory silica TLC using hexane/ CH_2Cl_2 (2/3) as the eluent. The pure product was obtained as a red powder from the top red band (15 mg, 14%). ^1H NMR: δ 7.94 (d, $J = 8 \text{ Hz}$, 4H, o-Ph-NO₂), 7.47–7.40 (m, 16H, o-PPh₂), 7.25–7.16 (m, 8H, p-PPh₂), 7.00–6.93 (m, 16H, m-PPh₂), 6.65 (d, $J = 8 \text{ Hz}$, 4H, m-Ph-NO₂), 2.62 (t, $J = 8$

Hz, 8H, dppe). $^{31}\text{P}\{\text{H}\}$ NMR: δ 52.0 (s). IR (Nujol, cm^{-1}): 2047 (m) $\nu(\text{Ru}-\text{C}\equiv\text{C})$.

*trans-Ru(C \equiv CC₆H₄C \equiv CSiMe₃-4)₂(dppe)₂ (3f).*²⁶ The TlCl precipitate was removed by filtration through neutral alumina (Brockmann I). The pure product was obtained from the filtrate as a pale yellow precipitate upon addition of Et₂O (96 mg, 81%). Single crystals suitable for X-ray diffraction were obtained from CH₂Cl₂/hexane. ^1H NMR: δ 7.52–7.43 (m, 16H, *o*-PPh₂), 7.25 (d, J = 8 Hz, 4H, C₂-Ph-C₂), 7.18–7.11 (m, 8H, *p*-PPh₂), 6.97–6.89 (m, 16H, *m*-PPh₂), 6.62 (d, J = 8 Hz, 4H, C₂-Ph-C₂), 2.66–2.58 (m, 8H, dppe), 0.26 (s, 9H, SiMe₃). $^{31}\text{P}\{\text{H}\}$ NMR: δ 53.4 (s, dppe). IR (Nujol, cm^{-1}): 2153 (m) $\nu(\text{C}\equiv\text{C})$; 2065 (s) $\nu(\text{Ru}-\text{C}\equiv\text{C})$.

*trans-Ru(C \equiv CC₆H₄C \equiv CCMe₃-4)₂(dppe)₂ (3g).*²⁶ The TlCl precipitate was removed by filtration through neutral alumina (Brockmann I). The pure product precipitated from the filtrate as pale yellow solids upon addition of Et₂O (96 mg, 83%). Single crystals suitable for X-ray diffraction were obtained from CHCl₃/MeOH. ^1H NMR: δ 7.52–7.43 (m, 16H, *o*-PPh₂), 7.20–7.10 (m, 12H, C₂-Ph-C₂/*p*-PPh₂), 6.96–6.88 (m, 16H, *m*-PPh₂), 6.63 (d, J = 8 Hz, 4H, C₂-Ph-C₂), 2.68–2.56 (m, 8H, dppe), 1.33 (s, 18H, CMe₃). $^{31}\text{P}\{\text{H}\}$ NMR: δ 52.5 (s, dppe). IR (Nujol, cm^{-1}): 2177 (w) $\nu(\text{C}\equiv\text{C})$; 2069 (s) $\nu(\text{Ru}-\text{C}\equiv\text{C})$.

*trans-Ru(C \equiv CC₆H₄C \equiv CH-4)₂(dppe)₂ (3i).*²⁷ 3f (30 mg, 0.023 mmol) was reacted with TBAF (1 M in THF, 46 μL , 0.046 mmol) in CH₂Cl₂ at room temperature overnight. The orange solution was filtered through neutral alumina (Brockmann I) and the filtrate taken to dryness to give the pure product as an orange powder (24 mg, 91%). Single crystals suitable for X-ray diffraction were obtained from CH₂Cl₂/hexane. ^1H NMR: δ 7.53–7.43 (m, 16H, *o*-PPh₂), 7.26 (d, J = 8 Hz, 4H, C₂-Ph-C₂), 7.20–7.13 (m, 8H, *p*-PPh₂), 6.99–6.89 (m, 16H, *m*-PPh₂), 6.64 (d, J = 8 Hz, 4H, C₂-Ph-C₂), 3.11 (s, 2H, C≡CH), 2.66–2.56 (m, 8H, dppe). $^{31}\text{P}\{\text{H}\}$ NMR: δ 52.6 (s, dppe). IR (Nujol, cm^{-1}): 3276 (s) $\nu(\text{C}\equiv\text{C}-\text{H})$; 2054 (w) $\nu(\text{Ru}-\text{C}\equiv\text{C})$.

Halide Abstractor Free Synthesis of *trans-Ru(C \equiv CC₆H₄R-4)₂(dppe)₂* (3c,h). To a solution of [RuCl(dppe)]OTf ([1]OTf, 0.100 g, 0.092 mmol) and DBU (excess) in CH₂Cl₂ (4 mL) was added the appropriate alkyne (0.20 mmol). The resulting solution was stirred at room temperature for 7 days. The yellow precipitate was removed by filtration and washed thoroughly with hexane. Product 3c was obtained as a yellow solid (47 mg, 44%); and 3h was obtained as an off-white powder (51 mg, 48%). Single crystals suitable for X-ray diffraction were obtained from CH₂Cl₂/hexane. ^1H NMR: δ 7.64–7.57 (m, 16H, *o*-PPh₂), 7.25–7.19 (m, 8H, *p*-PPh₂), 7.04–6.99 (m, 16H, *m*-PPh₂), 6.68 (d, J = 8 Hz, 4H, Ph-NH₂), 6.59 (d, J = 8 Hz, 4H, Ph-NH₂), 3.56 (s, 4H, NH₂), 2.73–2.61 (m, 8H, dppe). $^{31}\text{P}\{\text{H}\}$ NMR: δ 53.2 (s, dppe). IR (Nujol, cm^{-1}): 3351 (m) $\nu(\text{NH}_2)$, 2073 cm^{-1} $\nu(\text{C}\equiv\text{C})$. A trace amount of the monoacetylide 2h was detected in the ^{31}P NMR spectrum as a resonance near δ 49 ppm, which could not be removed due to the pronounced tendency of the sample toward decomposition (oxidation or protonation) in solution during recrystallization or column chromatography.

Synthesis of *trans-Ru(C \equiv CC₆H₄R¹-4)(C \equiv CC₆H₄R²-4)(dppe)₂ (4–6).* To a solution of the appropriate *trans-RuCl(C \equiv CC₆H₄R-4)(dppe)₂* (0.10 g) and DBU (excess) in CH₂Cl₂ (4 mL) was added TiBF₄ (1 equiv). Subsequent dropwise addition of HC≡CR' (1.1 equiv) dissolved in CH₂Cl₂ (\sim 3 mL) over 30 min generated an off-white precipitate (TlCl) that was removed by filtration. The final products were obtained from the yellow-orange filtrate after purification (vide infra).

trans-Ru(C \equiv CC₆H₄C \equiv CSiMe₃-4)(C \equiv CC₆H₄NH₂-4)(dppe)₂ (4). To a solution of 2f (0.100 g, 0.083 mmol) was added 4-ethynylaniline (0.012 g, 0.10 mmol) according to the general procedure. The TlCl precipitate was removed by filtration through basic alumina (Brockmann III). The pure product precipitated from the filtrate as orange solids upon addition of hexane (61 mg, 0.050 mmol, 60%). ^1H NMR: δ 7.67–7.60 (m, 8H, *o*-PPh₂), 7.39–7.34 (m, 8H, *o*-PPh₂), 7.23 (d, J = 8 Hz, 2H, *o*-Ph-TMSA), 7.20–7.09 (m, 8H, *p*-PPh₂), 7.20–7.09 (m, 8H, *m*-PPh₂), 7.00–6.93 (m, 8H, *m*-PPh₂), 6.68 (d, J = 8 Hz, 2H, Ph-NH₂), 6.56 (m, 2H, *m*-Ph-TMSA), 6.53 (d, J = 8 Hz, 2H, Ph-NH₂) 3.51 (s, 2H, NH₂), 2.65–2.58 (m, 8H, dppe), 0.26 (s, 9H, SiMe₃).

$^{31}\text{P}\{\text{H}\}$ NMR: δ 52.8 (s, dppe). IR (Nujol, cm^{-1}): $\nu(\text{NH}_2)$ not observed; 2151 (w) $\nu(\text{C}\equiv\text{C})$; 2062 (s) $\nu(\text{Ru}-\text{C}\equiv\text{C})$. Anal. Calcd: C, 72.32; H, 5.57; N, 1.15. Found: C, 72.51; H, 5.65; N, 1.29.

trans-Ru(C \equiv CC₆H₄CO₂Me-4)(C \equiv CC₆H₄NH₂-4)(dppe)₂ (5). To a solution of 2d (0.100 g, 0.092 mmol) was added 4-ethynylaniline (0.012 g, 0.10 mmol) according to the general procedure. The TlCl precipitate was removed by filtration through basic alumina (Brockmann III). The pure product precipitated from the filtrate as yellow solids upon addition of hexane and was washed with Et₂O (50 mg, 0.043 mmol, 47%). ^1H NMR: δ 7.79 (d, J = 8 Hz, 2H, *o*-Ph-CO₂Me), 7.70–7.58 (m, 8H, *o*-PPh₂), 7.41–7.32 (m, 8H, *o*-PPh₂), 7.16 (m, 8H, *p*-PPh₂), 7.01–6.95 (m, 8H, *m*-PPh₂), 6.95–6.88 (m, 8H, *m*-PPh₂), 6.69 (d, J = 8 Hz, 2H, Ph-NH₂), 6.64 (d, J = 8 Hz, 2H, *m*-Ph-CO₂Me), 6.54 (d, J = 8 Hz, 2H, Ph-NH₂), 3.90 (s, 3H, COO-Me), 3.52 (s br, 2H, NH₂), 2.66–2.58 (m, 8H, dppe). $^{31}\text{P}\{\text{H}\}$ NMR: δ 52.8 (s, dppe). IR (Nujol, cm^{-1}): $\nu(\text{NH}_2)$ not observed; 2058 $\nu(\text{Ru}-\text{C}\equiv\text{C})$. Anal. Calcd: C, 71.59; H, 5.24; N, 1.19. Found: C, 71.58; H, 5.26; N, 1.21.

trans-Ru(C \equiv CC₆H₄CO₂Me-4)(C \equiv CC₆H₄OMe-4)(dppe)₂ (6). To a solution of 2d (0.100 g, 0.092 mmol) was added 1-ethynyl-4-methoxybenzene (0.013 g, 0.10 mmol) according to the general procedure. The TlCl precipitate was removed by filtration through basic alumina (Brockmann III). The pure product precipitated from the filtrate as bright yellow solids upon addition of hexane (95 mg, 0.080 mmol, 87%). ^1H NMR: δ 7.79 (d, J = 8 Hz, 2H, *o*-Ph-CO₂Me), 7.65–7.59 (m, 8H, *o*-PPh₂), 7.41–7.35 (m, 8H, *o*-PPh₂), 7.21–7.12 (m, 8H, *p*-PPh₂), 7.01–6.95 (m, 8H, *m*-PPh₂), 6.95–6.89 (m, 8H, *m*-PPh₂), 6.79–6.71 (m, 4H, *o*/*m*-Ph-OMe), 6.65 (d, J = 8 Hz, 2H, *m*-Ph-CO₂Me), 3.90 (s, 4H, COO-Me), 3.81 (s, 4H, O-Me), 2.66–2.58 (t, J = 7 Hz, 8H, dppe). $^{31}\text{P}\{\text{H}\}$ NMR: δ 52.8 (s, dppe). IR (Nujol, cm^{-1}): 2060 $\nu(\text{Ru}-\text{C}\equiv\text{C})$; 1704 $\nu(\text{C}=\text{O})$. Anal. Calcd: C, 71.70; H, 5.26. Found: C, 71.66; H, 5.47.

Computational Details. Calculations have been carried out on the full complexes 3f,h, 4, and 5 in their neutral and cationic forms. Structure optimizations and frequency analyses were performed at DFT levels (see below), using a version of the TURBOMOLE 6.4⁶⁷ code locally modified by the Berlin group. Additional single-point TDDFT calculations were carried out employing the Gaussian09 code, as these match the experimental values more closely.⁶⁸ The computational protocol used has been developed specifically to handle the question of delocalization/localization of spin density and charge in organic^{69,70} and transition-metal mixed-valence systems,^{60,61,64,71} and it is known to generally provide accurate ground- and excited-state properties also for related open-shell systems. The approach is based on the adjusted global hybrid functional BLYP35,⁶⁹ which was constructed analogously to the B1LYP model,⁷² in conjunction with polarizable continuum solvent models. While not a thermochemically optimized functional, BLYP35 has been shown to provide a good balance between reduced self-interaction errors and a simulation of nondynamical correlation. In the present work, CH₂Cl₂ (permittivity ϵ = 8.93) was considered by the conductorlike screening solvent model (COSMO)⁷³ and by the closely related C-PCM model^{74,75} in the Gaussian09 TDDFT calculations. Notably, the TDDFT calculations took into account nonequilibrium solvation.^{76,77}

For all calculations, def2-SVP split-valence basis sets on the lighter atoms and the associated Stuttgart effective-core potentials with a corresponding def2-SVP valence basis for ruthenium were employed.^{78–80} An empirical scaling factor of 0.95 was applied to calculated harmonic vibrational frequencies.^{56,57} Additionally, computed IR stick spectra were convoluted with Gaussian broadening (σ = 15 cm^{-1}) using the Q-Spector program for better comparison with experimental IR spectra.⁸¹

For [3h]^{•+}, a two-dimensional relaxed scan of the PES with a fixed torsion angle θ between the plane of the aromatic ethynyl substituent and the plane bisecting the dppe ligands (Figure 3) and a fixed dihedral angle Ω (Figure 7) (which defines the relative conformation of the phenyl rings of the two C≡CC₆H₄NH₂-4 ligands) was performed. Starting from the structure obtained from a full optimization, both dihedral angles were varied in steps of 10°, from 0 to 90°. For convenience, the C₄–C₃–Ru₁–P₁ dihedral angle (Figure

3) was varied from 40 to 130° in the relaxed scan and afterward translated into θ , giving values between −3° and 89°.

Spin densities are plotted as isosurfaces (with values ± 0.002 au), using light gray for positive and red for negative values. Similarly, molecular orbitals are presented as isosurface plots (± 0.03 au) using light gray and blue colors for positive and negative signs, respectively. In the ball and stick plots, the atoms are also color-coded (ruthenium, yellow; phosphorus, green; carbon, gray; nitrogen and silicon, blue; oxygen, red; hydrogen, white). These plots were done with the Molekul program.⁸²

Crystallography. Single-crystal X-ray data for all of the compounds (except 2i) were collected at 120.0 K on a Bruker SMART 6000 diffractometer using graphite-monochromated Mo K α radiation ($\lambda = 0.71073$ Å). The data for compound 2i were collected at 120.0 K on a Rigaku Saturn 724+ diffractometer at station I19 of the Diamond Light Source synchrotron (undulator, $\lambda = 0.6889$ Å, ω -scan, 1.0°/frame) and processed using Bruker APEXII software. In all cases the sample temperature was controlled by Cryostream (Oxford Cryosystems) open-flow nitrogen cryostats. The structures were solved by direct methods and refined by full-matrix least squares on F^2 for all data using SHELXTL⁸³ and OLEX2⁸⁴ software. All non-disordered non-hydrogen atoms were refined with anisotropic displacement parameters; H atoms were placed in calculated positions and refined in the riding mode. Crystallographic data for the structures have been deposited with the Cambridge Crystallographic Data Centre as supplementary publications CCDC 991138–991149.

Crystal data for 2f: $C_{65}H_{61}ClP_4RuSi\cdot 1.5CH_2Cl_2$, $M_r = 1258.02$, triclinic, space group $P\bar{1}$, $a = 13.4989(4)$ Å, $b = 14.8937(4)$ Å, $c = 17.8696(5)$ Å, $\alpha = 113.42(1)$ °, $\beta = 98.65(1)$ °, $\gamma = 103.32(1)$ °, $U = 3088.00(15)$ Å 3 , $F(000) = 1298$, $Z = 2$, $D_{\text{calc}} = 1.356$ Mg/m 3 , $\mu = 0.590$ mm $^{-1}$, 37101 reflections collected, yielding 15588 unique data ($R_{\text{int}} = 0.1044$), final conventional R1(F) = 0.0627 for 8812 reflections with $I \geq 2\sigma$, wR2(F^2) = 0.1132 for all data (699 refined parameters), GOF = 1.012.

Crystal data for 2g: $C_{66}H_{61}ClP_4Ru$, $M_r = 1114.55$, triclinic, space group $P\bar{1}$, $a = 9.2573(4)$ Å, $b = 12.9014(6)$ Å, $c = 13.6270(7)$ Å, $\alpha = 63.759(1)$ °, $\beta = 71.267(1)$ °, $\gamma = 80.429(1)$ °, $U = 1381.88(11)$ Å 3 , $F(000) = 578$, $Z = 1$, $D_{\text{calc}} = 1.339$ Mg/m 3 , $\mu = 0.489$ mm $^{-1}$, 18235 reflections collected, yielding 15422 unique data ($R_{\text{int}} = 0.0195$), final conventional R1(F) = 0.0412 for 13757 reflections with $I \geq 2\sigma$, wR2(F^2) = 0.1099 for all data (641 refined parameters), GOF = 1.081.

Crystal data for 2i: $C_{62}H_{53}ClP_4Ru$, $M_r = 1058.44$, monolinic, space group $P2_1/c$, $a = 11.5037(7)$ Å, $b = 22.4968(8)$ Å, $c = 19.4374(10)$ Å, $\beta = 94.037(6)$ °, $U = 5017.9(4)$ Å 3 , $F(000) = 2184.0$, $Z = 4$, $D_{\text{calc}} = 1.401$ Mg/m 3 , $\mu = 0.534$ mm $^{-1}$, 53556 reflections collected, yielding 13451 unique data ($R_{\text{int}} = 0.0386$), final conventional R1(F) = 0.0376 for 11213 reflections with ($I \geq 2\sigma$), wR2(F^2) = 0.0987 for all data (613 refined parameters), GOF = 1.091.

Crystal data for 3a: $C_{70}H_{62}P_4Ru$, $M_r = 1128.15$, triclinic, space group $P\bar{1}$, $a = 9.4458(4)$ Å, $b = 12.9907(6)$ Å, $c = 13.5890(6)$ Å, $\alpha = 117.314(1)$ °, $\beta = 94.871(1)$ °, $\gamma = 104.724(1)$ °, $U = 1392.94(11)$ Å 3 , $F(000) = 586.0$, $Z = 1$, $D_{\text{calc}} = 1.345$ Mg/m 3 , $\mu = 0.440$ mm $^{-1}$, 16041 reflections collected, yielding 7679 unique data ($R_{\text{int}} = 0.0321$), final conventional R1(F) = 0.0397 for 6410 reflections with $I \geq 2\sigma$, wR2(F^2) = 0.1078 for all data (341 refined parameters), GOF = 1.056.

Crystal data for 3b: $C_{78}H_{78}P_4Ru\cdot 2CHCl_3$, $M_r = 1479.09$, triclinic, space group $P\bar{1}$, $a = 9.6718(2)$ Å, $b = 13.2334(3)$ Å, $c = 15.1804(4)$ Å, $\alpha = 78.10(1)$ °, $\beta = 77.00(1)$ °, $\gamma = 72.33(1)$ °, $U = 1783.81(7)$ Å 3 , $F(000) = 766.0$, $Z = 1$, $D_{\text{calc}} = 1.377$ Mg/m 3 , $\mu = 0.578$ mm $^{-1}$, 31919 reflections collected, yielding 10417 unique data ($R_{\text{int}} = 0.0498$), final conventional R1(F) = 0.0330 for 7985 reflections with ($I \geq 2\sigma$), wR2(F^2) = 0.0750 for all data (572 refined parameters), GOF = 0.932.

Crystal data for 3c: $C_{70}H_{62}O_2P_4Ru\cdot C_7H_8$, $M_r = 1251.27$, triclinic, space group $P\bar{1}$, $a = 9.1943(4)$ Å, $b = 12.7621(5)$ Å, $c = 13.5658(6)$ Å, $\alpha = 76.576(1)$ °, $\beta = 89.853(1)$ °, $\gamma = 80.994(1)$ °, $U = 1528.27(11)$ Å 3 , $F(000) = 651.0$, $Z = 1$, $D_{\text{calc}} = 1.360$ Mg/m 3 , $\mu = 0.411$ mm $^{-1}$, 20100 reflections collected, yielding 8842 unique data ($R_{\text{int}} = 0.0243$), final conventional R1(F) = 0.0348 for 7693 reflections with $I \geq 2\sigma$, wR2(F^2) = 0.0934 for all data (518 refined parameters), GOF = 1.052.

Crystal data for 3d: $C_{72}H_{62}O_4P_4Ru\cdot C_7H_8$, $M_r = 1308.30$, triclinic, space group $P\bar{1}$, $a = 9.3908(3)$ Å, $b = 12.8371(4)$ Å, $c = 13.8661(4)$ Å, $\alpha = 97.95(1)$ °, $\beta = 108.73(1)$ °, $\gamma = 92.24(1)$ °, $U = 1561.58(8)$ Å 3 , $F(000) = 680.0$, $Z = 1$, $D_{\text{calc}} = 1.391$ Mg/m 3 , $\mu = 0.407$ mm $^{-1}$, 20792 reflections collected, yielding 9066 unique data ($R_{\text{int}} = 0.0440$), final conventional R1(F) = 0.0347 for 7020 reflections with $I \geq 2\sigma$, wR2(F^2) = 0.0714 for all data (539 refined parameters), GOF = 0.969.

Crystal data for 3f: $C_{78}H_{74}Si_2P_4Ru$, $M_r = 1292.50$, triclinic, space group $P\bar{1}$, $a = 9.4265(4)$ Å, $b = 13.5130(5)$ Å, $c = 14.2919(6)$ Å, $\alpha = 76.253(2)$ °, $\beta = 74.292(3)$ °, $\gamma = 71.596(2)$ °, $U = 1639.6(1)$ Å 3 , $F(000) = 674.0$, $Z = 1$, $D_{\text{calc}} = 1.309$ Mg/m 3 , $\mu = 0.417$ mm $^{-1}$, 18597 reflections collected, yielding 8224 unique data ($R_{\text{int}} = 0.0493$), final conventional R1(F) = 0.0453 for 7020 reflections with $I \geq 2\sigma$, wR2(F^2) = 0.1119 for all data (533 refined parameters), GOF = 0.990.

Crystal data for 3g: $C_{84}H_{78}Br_{0.1}Cl_2P_4Ru$, $M_r = 1745.80$, triclinic, space group $P\bar{1}$, $a = 10.8015(4)$ Å, $b = 12.4654(4)$ Å, $c = 16.4565(6)$ Å, $\alpha = 94.896(1)$ °, $\beta = 105.108(1)$ °, $\gamma = 103.004(1)$ °, $U = 2059.8(1)$ Å 3 , $F(000) = 894.0$, $Z = 1$, $D_{\text{calc}} = 1.407$ Mg/m 3 , $\mu = 0.749$ mm $^{-1}$, 35554 reflections collected, yielding 11468 unique data ($R_{\text{int}} = 0.0314$), final conventional R1(F) = 0.0429 for 9600 reflections with $I \geq 2\sigma$, wR2(F^2) = 0.1141 for all data (463 refined parameters), GOF = 1.083.

Crystal data for 3h: $C_{68}H_{60}N_2P_4Ru$, $M_r = 1130.13$, triclinic, space group $P\bar{1}$, $a = 9.3537(3)$ Å, $b = 12.9960(4)$ Å, $c = 13.4808(4)$ Å, $\alpha = 117.164(1)$ °, $\beta = 95.632(1)$ °, $\gamma = 103.708(1)$ °, $U = 1375.51(7)$ Å 3 , $F(000) = 586.0$, $Z = 1$, $D_{\text{calc}} = 1.364$ Mg/m 3 , $\mu = 0.446$ mm $^{-1}$, 17825 reflections collected, yielding 7635 unique data ($R_{\text{int}} = 0.0347$), final conventional R1(F) = 0.0390 for 6328 reflections with $I \geq 2\sigma$, wR2(F^2) = 0.0992 for all data (460 refined parameters), GOF = 1.041.

Crystal data for 3i: $C_{72}H_{58}P_4Ru\cdot CH_2Cl_2$, $M_r = 1233.06$, triclinic, space group $P\bar{1}$, $a = 9.6711(2)$ Å, $b = 12.9728(3)$ Å, $c = 23.8066(6)$ Å, $\alpha = 81.22(1)$ °, $\beta = 86.79(1)$ °, $\gamma = 83.99(1)$ °, $U = 2933.2(1)$ Å 3 , $F(000) = 1272.0$, $Z = 2$, $D_{\text{calc}} = 1.396$ Mg/m 3 , $\mu = 0.512$ mm $^{-1}$, 48867 reflections collected, yielding 15586 unique data ($R_{\text{int}} = 0.0528$), final conventional R1(F) = 0.0439 for 11224 reflections with $I \geq 2\sigma$, wR2(F^2) = 0.1156 for all data (724 refined parameters), GOF = 1.038.

ASSOCIATED CONTENT

Supporting Information

Text, figures, tables, and CIF and xyz files giving synthetic procedures for key ligands and precursors, plots of 1 H and 31 P NMR spectra of complexes, COSY spectra of complexes 4, crystallographic details, crystallographically determined bond lengths (Å) and angles (deg), plots showing comparison of IR spectroelectrochemical data and calculated vibrational frequencies, plots and NIR expansion of UV-vis/NIR spectroelectrochemical data, calculated energies, vibrational frequencies, orbital energies and spin-density distributions, and all computed molecule Cartesian coordinates in a format for convenient visualization. This material is available free of charge via the Internet at <http://pubs.acs.org>.

AUTHOR INFORMATION

Corresponding Authors

*M.K.: fax, +49 30 314 21075; tel, +49 30 314 79682; e-mail, martin.kaupp@tu-berlin.de.

*P.J.L. fax, +61 8 6488 7330; tel, +61 8 6488 3045; e-mail, paul.low@uwa.edu.au

Notes

The authors declare no competing financial interest.

ACKNOWLEDGMENTS

This work has been supported by the Berlin DFG cluster of excellence on “Unifying Concepts in Catalysis” (UniCat), by DFG project KA1187/13-1, by the EPSRC, and the ARC. We thank the Diamond Light Source for an award of instrument

time on the Station I19 (MT 6749) for collection the data for **2i** and the instrument scientists for support. M.P. gratefully acknowledges the German Academic Exchange Service (DAAD) for a travel scholarship. P.J.L. held an EPSRC Leadership Fellowship and currently holds an ARC Future Fellowship (FT120100073).

■ REFERENCES

- (1) Meng, F. B.; Hervault, Y. M.; Norel, L.; Costuas, K.; Van Dyck, C.; Geskin, V.; Cornil, J.; Hng, H. H.; Rigaut, S.; Chen, X. D. *Chem. Sci.* **2012**, *3*, 3113–3118.
- (2) Kim, B.; Beebe, J. M.; Olivier, C.; Rigaut, S.; Touchard, D.; Kushmerick, J. G.; Zhu, X. Y.; Frisbie, C. D. *J. Phys. Chem. C* **2007**, *111*, 7521–7526.
- (3) Rigaut, S. *Dalton Trans.* **2013**, *42*, 15859–15863.
- (4) Powell, C. E.; Humphrey, M. G. *Coord. Chem. Rev.* **2004**, *248*, 725–756.
- (5) Costuas, K.; Rigaut, S. *Dalton Trans.* **2011**, *40*, 5643–5658.
- (6) Benameur, A.; Brignou, P.; Di Piazza, E.; Hervault, Y. M.; Norel, L.; Rigaut, S. *New J. Chem.* **2011**, *35*, 2105–2113.
- (7) Rigaut, S.; Perruchon, J.; Le Pichon, L.; Touchard, D.; Dixneuf, P. H. *J. Organomet. Chem.* **2003**, *670*, 37–44.
- (8) McDonagh, A. M.; Powell, C. E.; Morrall, J. P.; Cifuentes, M. P.; Humphrey, M. G. *Organometallics* **2003**, *22*, 1402–1413.
- (9) Faulkner, C. W.; Ingham, S. L.; Khan, M. S.; Lewis, J.; Long, N. J.; Raithby, P. R. *J. Organomet. Chem.* **1994**, *482*, 139–145.
- (10) Gauthier, N.; Olivier, C.; Rigaut, S.; Touchard, D.; Roisnel, T.; Humphrey, M. G.; Paul, F. *Organometallics* **2008**, *27*, 1063–1072.
- (11) Olivier, C.; Kim, B.; Touchard, D.; Rigaut, S. *Organometallics* **2008**, *27*, 509–518.
- (12) Touchard, D.; Haquette, P.; Guesmi, S.; Le Pichon, L.; Daridor, A.; Toupet, L.; Dixneuf, P. H. *Organometallics* **1997**, *16*, 3640–3648.
- (13) West, P. J.; Cifuentes, M. P.; Schwich, T.; Randles, M. D.; Morrall, J. P.; Kulasekera, E.; Petrie, S.; Stranger, R.; Humphrey, M. G. *Inorg. Chem.* **2012**, *51*, 10495–10502.
- (14) Touchard, D.; Guesmi, S.; Le Pichon, L.; Daridor, A.; Dixneuf, P. H. *Inorg. Chim. Acta* **1998**, *280*, 118–124.
- (15) Younus, M.; Long, N. J.; Raithby, P. R.; Lewis, J.; Page, N. A.; White, A. J. P.; Williams, D. J.; Colbert, M. C. B.; Hodge, A. J.; Khan, M. S.; Parker, D. G. *J. Organomet. Chem.* **1999**, *578*, 198–209.
- (16) Atherton, Z.; Faulkner, C. W.; Ingham, S. L.; Kakkar, A. K.; Khan, M. S.; Lewis, J.; Long, N. J.; Raithby, P. R. *J. Organomet. Chem.* **1993**, *462*, 265–270.
- (17) Fox, M. A.; Harris, J. E.; Heider, S.; Perez-Gregorio, V.; Zakrzewska, M. E.; Farmer, J. D.; Yufit, D. S.; Howard, J. A. K.; Low, P. J. *J. Organomet. Chem.* **2009**, *694*, 2350–2358.
- (18) Fillaut, J. L.; Andries, J.; Marwaha, R. D.; Lanoe, P. H.; Lohio, O.; Toupet, L.; Williams, J. A. G. *J. Organomet. Chem.* **2008**, *693*, 228–234.
- (19) Powell, C. E.; Hurst, S. K.; Morrall, J. P.; Cifuentes, M. P.; Roberts, R. L.; Samoc, M.; Humphrey, M. G. *Organometallics* **2007**, *26*, 4456–4463.
- (20) Koutsantonis, G. A.; Jenkins, G. I.; Schauer, P. A.; Szczepaniak, B.; Skelton, B. W.; Tan, C.; White, A. H. *Organometallics* **2009**, *28*, 2195–2205.
- (21) Li, Z. H.; Beatty, A. M.; Fehlner, T. P. *Inorg. Chem.* **2003**, *42*, 5707–5714.
- (22) Khairul, W. M.; Fox, M. A.; Zaitseva, N. N.; Gaudio, M.; Yufit, D. S.; Skelton, B. W.; White, A. H.; Howard, J. A. K.; Bruce, M. I.; Low, P. J. *Dalton Trans.* **2009**, *610*–620.
- (23) Hurst, S. K.; Cifuentes, M. P.; McDonagh, A. M.; Humphrey, M. G.; Samoc, M.; Luther-Davies, B.; Asselberghs, I.; Persoons, A. J. *Organomet. Chem.* **2002**, *642*, 259–267.
- (24) Lavastre, O.; Plass, J.; Bachmann, P.; Guesmi, S.; Moinet, C.; Dixneuf, P. H. *Organometallics* **1997**, *16*, 184–189.
- (25) Klein, A.; Lavastre, O.; Fiedler, J. *Organometallics* **2006**, *25*, 635–643.
- (26) Marques-Gonzalez, S.; Yufit, D. S.; Howard, J. A. K.; Martin, S.; Osorio, H. M.; Garcia-Suarez, V. M.; Nichols, R. J.; Higgins, S. J.; Cea, P.; Low, P. J. *Dalton Trans.* **2013**, *42*, 338–341.
- (27) Lavastre, O.; Even, M.; Dixneuf, P. H.; Pacreau, A.; Vairon, J. P. *Organometallics* **1996**, *15*, 1530–1531.
- (28) Dalton, G. T.; Cifuentes, M. P.; Watson, L. A.; Petrie, S.; Stranger, R.; Samoc, M.; Humphrey, M. G. *Inorg. Chem.* **2009**, *48*, 6534–6547.
- (29) Ouerfelli, I.; Gatri, R.; Efrit, M. L.; Dua, N.; Perruchon, J.; Golhen, S.; Toupet, L.; Fillaut, J. L. *J. Organomet. Chem.* **2011**, *696*, 670–675.
- (30) Gauthier, N.; Tchouar, N.; Justaud, F.; Argouarch, G.; Cifuentes, M. P.; Toupet, L.; Touchard, D.; Halet, J. F.; Rigaut, S.; Humphrey, M. G.; Costuas, K.; Paul, F. *Organometallics* **2009**, *28*, 2253–2266.
- (31) Hurst, S. K.; Cifuentes, M. P.; Morrall, J. P. L.; Lucas, N. T.; Whittall, I. R.; Humphrey, M. G.; Asselberghs, I.; Persoons, A.; Samoc, M.; Luther-Davies, B.; Willis, A. C. *Organometallics* **2001**, *20*, 4664–4675.
- (32) Fillaut, J. L.; Perruchon, J.; Blanchard, P.; Roncali, J.; Golhen, S.; Allain, M.; Migalsaka-Zalas, A.; Kityk, I. V.; Sahraoui, B. *Organometallics* **2005**, *24*, 687–695.
- (33) Morrall, J. P. L.; Cifuentes, M. P.; Humphrey, M. G.; Kellens, R.; Robijns, E.; Asselberghs, I.; Clays, K.; Persoons, A.; Samoc, M.; Willis, A. C. *Inorg. Chim. Acta* **2006**, *359*, 998–1005.
- (34) Grelaud, G.; Cifuentes, M. P.; Schwich, T.; Argouarch, G.; Petrie, S.; Stranger, R.; Paul, F.; Humphrey, M. G. *Eur. J. Inorg. Chem.* **2012**, *65*–75.
- (35) Trujillo, A.; Fuentealba, M.; Arratia-Perez, R.; Howard, J. A. K. *Acta Crystallogr., Sect. E: Struct. Rep. Online* **2012**, *68*, m1445.
- (36) Low, P. J. *Coord. Chem. Rev.* **2013**, *257*, 1507–1532.
- (37) Bruce, M. I.; Buschel, S.; Cole, M. L.; Scoleri, N.; Skelton, B. W.; White, A. H.; Zaitseva, N. N. *Inorg. Chim. Acta* **2012**, *382*, 6–12.
- (38) Wuttke, E.; Pevny, F.; Hervault, Y. M.; Norel, L.; Drescher, M.; Winter, R. F.; Rigaut, S. *Inorg. Chem.* **2012**, *51*, 1902–1915.
- (39) Anderson, J. N.; Brookes, N. J.; Coe, B. J.; Coles, S. J.; Light, M. E.; Hursthorne, M. B. *Acta Crystallogr., Sect. C* **2003**, *59*, M215–M217.
- (40) Jeffery, C. J.; Cifuentes, M. P.; Dalton, G. T.; Corkery, T. C.; Randles, M. D.; Willis, A. C.; Samoc, M.; Humphrey, M. G. *Macromol. Rapid Commun.* **2010**, *31*, 846–849.
- (41) Gauthier, N.; Argouarch, G.; Paul, F.; Toupet, L.; Ladjaraf, A.; Costuas, K.; Halet, J. F.; Samoc, M.; Cifuentes, M. P.; Corkery, T. C.; Humphrey, M. G. *Chem. Eur. J.* **2011**, *17*, 5561–5577.
- (42) Vacher, A.; Barriere, F.; Roisnel, T.; Piekara-Sady, L.; Lorcy, D. *Organometallics* **2011**, *30*, 3570–3578.
- (43) Lebreton, C.; Touchard, D.; Le Pichon, L.; Daridor, A.; Toupet, L.; Dixneuf, P. H. *Inorg. Chim. Acta* **1998**, *272*, 188–196.
- (44) Norel, L.; Bernot, K.; Feng, M.; Roisnel, T.; Caneschi, A.; Sessoli, R.; Rigaut, S. *Chem. Commun.* **2012**, *48*, 3948–3950.
- (45) Wuttke, E.; Hervault, Y. M.; Polit, W.; Linseis, M.; Erler, P.; Rigaut, S.; Winter, R. F. *Organometallics* **2014**, DOI: 10.1021/om400642j.
- (46) McGrady, J. E.; Lovell, T.; Stranger, R.; Humphrey, M. G. *Organometallics* **1997**, *16*, 4004–4011.
- (47) Lever, A. B. P. *Inorg. Chem.* **1990**, *29*, 1271–1285.
- (48) Heath, G. A.; Humphrey, D. G. *J. Chem. Soc., Chem. Commun.* **1991**, 1668–1671.
- (49) McDonagh, A. M.; Whittall, I. R.; Humphrey, M. G.; Hockless, D. C. R.; Skelton, B. W.; White, A. H. *J. Organomet. Chem.* **1996**, *523*, 33–40.
- (50) Pombeiro, A. J. L. *J. Organomet. Chem.* **2005**, *690*, 6021–6040.
- (51) Powell, C. E.; Cifuentes, M. P.; Morrall, J. P.; Stranger, R.; Humphrey, M. G.; Samoc, M.; Luther-Davies, B.; Heath, G. A. *J. Am. Chem. Soc.* **2003**, *125*, 602–610.
- (52) Pevny, F.; Di Piazza, E.; Norel, L.; Drescher, M.; Winter, R. F.; Rigaut, S. *Organometallics* **2010**, *29*, 5912–5918.
- (53) Green, K. A.; Cifuentes, M. P.; Corkery, T. C.; Samoc, M.; Humphrey, M. G. *Angew. Chem., Int. Ed.* **2009**, *48*, 7867–7870.
- (54) Low, P. J.; Bock, S. *Electrochim. Acta* **2013**, *110*, 681–692.

- (55) Fox, M. A.; Roberts, R. L.; Khairul, W. M.; Hartl, F.; Low, P. J. *J. Organomet. Chem.* **2007**, *692*, 3277–3290.
- (56) Roder, J. C.; Meyer, F.; Hyla-Kryspin, I.; Winter, R. F.; Kaifer, E. *Chem.—Eur. J.* **2003**, *9*, 2636–2648.
- (57) Scott, A. P.; Radom, L. *J. Phys. Chem.* **1996**, *100*, 16502–16513.
- (58) The contributions for **4a,b** sum to more than 100%, due to rounding of contributions and negative contributions to the spin density due to spin polarization.
- (59) Jones, S. C.; Coropceanu, V.; Barlow, S.; Kinnibrugh, T.; Timofeeva, T.; Bredas, J. L.; Marder, S. R. *J. Am. Chem. Soc.* **2004**, *126*, 11782–11783.
- (60) Parthey, M.; Vincent, K. B.; Renz, M.; Schauer, P. A.; Yufit, D. S.; Howard, J. A. K.; Kaupp, M.; Low, P. J. *Inorg. Chem.* **2014**, *53*, 1544–1554.
- (61) Parthey, M.; Gluyas, J. B. G.; Fox, M. A.; Low, P. J.; Kaupp, M. *Chem. Eur. J.* **2014**, *20*, 6895–6908.
- (62) Costuas, K.; Cadot, O.; Justaud, F.; Le Stang, S.; Paul, F.; Monari, A.; Evangelisti, S.; Toupet, L.; Lapinte, C.; Halet, J. F. *Inorg. Chem.* **2011**, *50*, 12601–12622.
- (63) Fitzgerald, E. C.; Ladjarafi, A.; Brown, N. J.; Collison, D.; Costuas, K.; Edge, R.; Halet, J. F.; Justaud, F.; Low, P. J.; Meghezzi, H.; Roisnel, T.; Whiteley, M. W.; Lapinte, C. *Organometallics* **2011**, *30*, 4180–4195.
- (64) Parthey, M.; Gluyas, J. B. G.; Schauer, P. A.; Yufit, D. S.; Howard, J. A. K.; Kaupp, M.; Low, P. J. *Chem. Eur. J.* **2013**, *19*, 9780–9784.
- (65) Pascal, P. *Nouveau Traité de Chimie Minearle*. Masson-Paris, Vol VI, p. 92 **1961**.
- (66) Krejcik, M.; Danek, M.; Hartl, F. *J. Electroanal. Chem.* **1991**, *317*, 179–187.
- (67) TURBOMOLE (V6.4 2012); University of Karlsruhe and Forschungszentrum Karlsruhe GmbH, TURBOMOLE GmbH since 2007.
- (68) Frisch, M. J., et al. *Gaussian 09; Revision A.02*; Gaussian Inc., Wallingford, CT, 2009.
- (69) Renz, M.; Theilacker, K.; Lambert, C.; Kaupp, M. *J. Am. Chem. Soc.* **2009**, *131*, 16292–16302.
- (70) Renz, M.; Kess, M.; Diedenhofen, M.; Klamt, A.; Kaupp, M. *J. Chem. Theory Comput.* **2012**, *8*, 4189–4203.
- (71) Vincent, K. B.; Zeng, Q.; Parthey, M.; Yufit, D. S.; Howard, J. A. K.; Hartl, F.; Kaupp, M.; Low, P. J. *Organometallics* **2013**, *32*, 6022–6032.
- (72) Adamo, C.; Barone, V. *Chem. Phys. Lett.* **1997**, *274*, 242–250.
- (73) Klamt, A.; Schuurmann, G. *J. Chem. Soc., Perkin Trans. 2* **1993**, 799–805.
- (74) Cossi, M.; Rega, N.; Scalmani, G.; Barone, V. *J. Comput. Chem.* **2003**, *24*, 669–681.
- (75) Barone, V.; Cossi, M. *J. Phys. Chem. A* **1998**, *102*, 1995–2001.
- (76) Klamt, A. *J. Phys. Chem.* **1996**, *100*, 3349–3353.
- (77) Scalmani, G.; Frisch, M. J.; Mennucci, B.; Tomasi, J.; Cammi, R.; Barone, V. *J. Chem. Phys.* **2006**, *124*, 094107.
- (78) Weigend, F.; Ahlrichs, R. *Phys. Chem. Chem. Phys.* **2005**, *7*, 3297–3305.
- (79) Schafer, A.; Horn, H.; Ahlrichs, R. *J. Chem. Phys.* **1992**, *97*, 2571–2577.
- (80) Andrae, D.; Hausermann, U.; Dolg, M.; Stoll, H.; Preuss, H. *Theor. Chim. Acta* **1990**, *77*, 123–141.
- (81) Pelmenschikov, V.; Guo, Y. S.; Wang, H. X.; Cramer, S. P.; Case, D. A. *Faraday Discuss.* **2011**, *148*, 409–420.
- (82) Varetto, I. MOLEKEL 5.4; Swiss National Supercomputing Centre, Manno, Switzerland.
- (83) Sheldrick, G. M. *Acta Crystallogr., Sect. A* **2008**, *64*, 112–122.
- (84) Dolomanov, O. V.; Bourhis, L. J.; Gildea, R. J.; Howard, J. A. K.; Puschmann, H. *J. Appl. Crystallogr.* **2009**, *42*, 339–341.